Journal Pre-proof

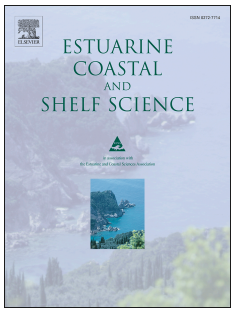

Investigation of 3D circulation and secondary flows in the St. Lawrence Fluvial Estuary at a tidal junction

M. Le Mouel, P. Matte, A. Hammouti, D. Pham Van Bang

PII: S0272-7714(24)00446-3

DOI: https://doi.org/10.1016/j.ecss.2024.109058

Reference: YECSS 109058

To appear in: *Estuarine, Coastal and Shelf Science*

Received Date: 15 August 2024

Revised Date: 1 November 2024

Accepted Date: 20 November 2024

Please cite this article as: Le Mouel, M., Matte, P., Hammouti, A., Pham Van Bang, D., Investigation of 3D circulation and secondary flows in the St. Lawrence Fluvial Estuary at a tidal junction, *Estuarine, Coastal and Shelf Science*, https://doi.org/10.1016/j.ecss.2024.109058.

Investigation of 3D circulation and secondary flows in the St. Lawrence Fluvial Estuary at a tidal junction

Authors : M. Le Mouel[1,3], P. Matte[2], A. Hammouti[1,3], D. Pham Van Bang[1,3*]

[1]: Department of Construction Engineering, Ecole de Technologie Supérieure (ETS), Université du Québec, 1100 rue Notre-Dame Ouest, Montréal (QC) H3C 1K3, Canada

[2]: Meteorological Research Division, Environment and Climate Change Canada, Quebec City (QC), Canada

[3]: Environmental Hydraulic Laboratory, Institut National de la Recherche Scientifique (INRS), 490 rue de la Couronne, Québec (QC), Canada[*] : corresponding author : damien.pham-van-bang@etsmtl.ca

Abstract

To enhance understanding of the complex functioning of the St. Lawrence fluvial estuary—a macro-tidal, freshwater estuary located in Quebec, Canada—a 3D numerical model is set up to investigate its hydrodynamics. Validation of the 3D model used field data on water levels, discharge rates, and velocities during both neap and spring tide periods. Comparison of the model with existing 2DH results illustrates the 3D model's ability to represent the time evolution of the secondary flow during tidal forcing in the confluence/divergence zone around Île d'Orléans. 3D results highlight the great importance of the vertical component of velocity in studying a site with complex geometry. A more detailed analysis of velocities and turbulence at the Île d'Orléans junction shows a time lag of around 1h between current slack and the tidal slack. On the one hand, the current reverses earlier at the bank level than in the deep channel during both ebb and flood periods. On the other hand, the current reverses more quickly at the bottom than at the surface in the main channel. Site geometry, friction and the presence of return currents are the main factors explaining this. This paper highlights the importance of 3D modeling for gaining a deeper understanding of estuarine dynamics, even in the tidal freshwater zone, revealing processes ignored by 2D depth integrated models. Such modeling can assist in planning future field measurement campaigns and improve space-time interpolation methods for velocities in wide estuaries. Additionally, it provides a solid foundation for studying couplings (chemical or particulate) and making predictions, particularly in the context of climate change.

Keyword

3D numerical modeling, hydrodynamic, St. Lawrence fluvial estuary, tidal junction, secondary flows, fortnightly cycles

1. Introduction

Estuaries are complex systems, situated at the interface between fresh and salt water, and subject to the influence of river discharge and tidal forces. The variability and nonlinear interactions between factors such as currents, turbulence, tides, river flow, salinity, sediment dynamics, temperature and geometry give rise to dynamic behaviors that are challenging to comprehend. The additional complexity introduced by spatio-temporal variations and sensitivity to meteorological and anthropogenic conditions further complicates their analysis. In order to fully grasp these phenomena, a three-dimensional (3D) analysis is essential, as it captures vertical, horizontal and temporal evolutions, thereby providing a more comprehensive view of estuarine dynamics. This study aims to achieve a thorough understanding of the 3D circulation and secondary flows in the St. Lawrence fluvial estuary (SLFE) at a tidal junction through numerical modeling.

A tidal junction, also known as a tidal convergence zone, is a critical area in coastal and estuarine environments where different tidal regimes intersect. These junctions are characterized by complex hydrodynamic interactions resulting from the confluence/diffluence of tidal currents, often leading to enhanced mixing and turbulent energy dissipation. Understanding the dynamics of tidal junctions is crucial for coastal engineering and management, as these areas are often hotspots for erosion, sediment deposition, and habitat formation. Advanced numerical modeling [1] and field observations [2], including the use of Acoustic Doppler Current Profilers (ADCP), are essential tools in studying these intricate processes, enabling researchers to predict and mitigate the impacts of human activities and climate change on these sensitive environments.

Over the past 50 years, numerous mathematical and numerical models of the St. Lawrence Estuary (SLE) have been developed, facilitating longitudinal analyses of the estuary. Initially, one-dimensional (1D) models were developed for the entire SLE to study tidal propagation under the combined effects of convergence and friction [3], [4], [5], [6], [7], [8], [9], [10], [11], [12], [13], [14], [15]. The use of numerical models was then extended to estimate flows and study time evolution of salinity under tidal flows ([11], [16], [17]). However, these 1D models have limitations: the Upper Estuary was poorly studied and the complex geometry was oversimplified, making these 1D-models unable to describe saline intrusion in the estuary.

Vertical, width-averaged (2DV) models have been developed for the SLE. In these models, Coriolis effects are not considered [18], [19]. However, 2DV models with a more complex bathymetry [20] provide valuable insights into the vertical processes responsible for salinity intrusion and stratification in the SLE. Additionally, horizontal, depth-integrated (2DH) numerical models have been developed for the SLE, based on the so-called shallow water equations. This 2DH formulation is suitable for considering Coriolis effects and residual and tidal currents in the SLE [4], [9], [14], [21], [22], [23].

More recent studies using 2D shallow water models have focused on tidal flow analysis in the SLFE [24] coastal flooding of Quebec City [25], hydrokinetic power assessment of SLE [26] or hydrodynamic

coupling with wind and ice [27]. However, these 2D models cannot capture the internal behaviors of estuarine circulation or flow stratification. These limitations are critical in the SLFE, which features strong confluences, large islands and deep canyons.

The previously mentioned limitations of earlier 1D, 2DV or 2DH models highlight the necessity of developing a full 3D approach to accurately represent the estuary's fully 3D geometry and dynamics. The first application of a 3D model in the SLE was by Gagnon [28] to study tidal propagation. Subsequent 3D models have enhanced understanding of the formation and circulation processes of water masses, particularly in relation to winter ice melt and salinity in the Lower Estuary and the Gulf of St. Lawrence ([29], [30], [31], [32]). The 3D flow model of the SLE by Saucier et al.(2009) [31] was also used to create the Atlas of tidal currents of Canadian Hydrographic Service [33], which had a horizontal resolution of 400m. Other 3D model applications in the SLE have ranged from local-scale studies of nonlinear internal waves in the North Channel [34] to global-scale studies of the Gulf with coarse resolution to examine biological species and Lagrangian coherent structures ([35], [36], [37], [38], [39]). The CIOPS-E forecasting system [40] uses a one-way downscaling technique with a ~2 km-resolution horizontal grid to simulate ice and ocean conditions over the northwest Atlantic Ocean up to Quebec City, which is not precise enough to describe the dynamics in the local region at the tidal junction near Quebec city. STLE500 and STLE200 [41] represent the most recent versions of the 3D model of the estuary, the most advanced 3D system known to us on a regular grid. However, a fixed grid is unsuitable relative to computational cost for the local study at a flow junction under the effect of an intense river discharge and high tidal range, which require a flexible mesh to attain very high spatial resolution in the vicinity of man-made structures, complex coastlines and sharp bathymetric gradients.

Few studies have focused on the fluvial (freshwater) part of the SLE estuary due to its highly complex geometry, characterized by strong convergence, large islands, and multiple deep submarine canyons. These features require an unstructured computational mesh with local refinements and a robust algorithm to accurately simulate secondary flows. Furthermore, the SLFE is a dynamic region presenting many environmental issues associated with sediment dynamics, salinity intrusion and navigation. The development of a new 3D numerical model with optimal resolution enables an updated understanding of 3D flow dynamics in the SLFE, leveraging the latest advances in the TELEMAC 3D open-source modeling system. For the first time, this study uses ADCP measurement from the field campaign by Matte et al. (2014) [42], which provides a unique high-resolution dataset covering the entire SLFE, to describe the 3D flow pattern in the diffluence/confluence zone of Île d'Orléans under tidal forcing.

In addition, close to this area characterized by recirculation [43] are the main wastewater dischargers of the City of Quebec and the drinking water intakes of the cities of Lévis and Quebec. Thus, the 3D approach proves particularly precious in view of diffuse or point-source pollution issues. Indeed, these complex circulations, including the vertical velocity component, can influence pollutant residence times and modify their diffusion in the environment ([44], [45], [46]). Other studies in the SLFE illustrate the

critical importance of 3D modeling in understanding these dynamics. They emphasize how tidal currents impact the vertical migration of zooplankton, revealing patterns of upward migration during flood tides and downward migration during ebb tides [47] —dynamics that are not captured by 2D models.

Some studies conducted direct comparisons between 2D and 3D models in various environments, including channels, lake systems, reservoirs, rivers, and coastal areas ([48], [49], [50], [51], [52], [53], [54]). However, few specifically focus on estuaries [55]. These comparisons reveal significant differences in the results produced by 2D and 3D models, particularly concerning specific parameters and the location and intensity of various phenomena ([48], [51], [54]). The inclusion of the vertical velocity component significantly impacts calculations of key parameters like shear stress, affecting sediment processes and habitat dynamics [48]. Discrepancies also arise in residence times and tracer transport ([51], [54]), which can be problematic, especially in pollution scenarios.

Ishikawa et al. (2022) showed that in a subtropical reservoir, 3D simulations were more accurate than 2D, particularly regarding flow velocities, density currents, and temperature gradients, highlighting the limitations of 2D models [51]. Furthermore, 3D models are often essential for capturing complex effects due to irregular geometries, such as steep dune slopes [49], anthropogenic structures [52] or pronounced bank curvatures [53], which can alter lateral and vertical flows [50], [53].

In estuaries, where many of these parameters and phenomena interact, comparing 2D and 3D models is relevant. Chen et al. (2012) found that in the Danshui Estuary, a 3D model more accurately represented water levels during high river discharge than a 2DV model [55]. However, no direct comparison between 2DH and 3D models was conducted in strongly tidal-influenced estuaries, especially at tidal junctions.

The aim of this study is to compare 2D and 3D numerical simulations of the hydrodynamics in the St. Lawrence fluvial estuary, which is characterized by complex bathymetry and tidal junction flow dynamics. The performance of the existing 2D numerical model [43], [56] and equivalent 2D results issued from the newly 3D developed model is evaluated against field measurements on flows and velocities analises during tidal cycles [57]. Besides, the fully 3D simulation results are used to extrapolate unmeasured hydrodynamic quantities and enhance our understanding of this specific environment. Particular attention is given to the behavior of the tidal junction, which is captured using a high-resolution numerical model where complex 3D flows occur. Finally, an in-depth analysis of the 3D hydrodynamics of the SLFE is carried out, focusing on residual lateral and transverse circulations, currents and turbulence, considering the fortnightly tidal cycle.

2. Study area

Originating from the great North American lakes, the St. Lawrence Estuary is one of the major shipping routes for international maritime trade with the United States and Europe. The estuary, in the strict sense, extends from Trois-Rivières to Pointe-des-Monts at its mouth. It separates the Appalachian

Mountains to the south from the Canadian Shield to the north and is divided into three distinct areas: the Fluvial Estuary, the Upper Estuary and the Lower Estuary (Fig. 1).

The flow in the St. Lawrence River fluctuates seasonally, reaching a minimum of 7,000 m^3/s (March 1965) and a maximum of 32,700 m^3/s (April 1976), with an average annual flow of 12,200 m^3/s at Quebec City during the 1960-2010 period [58]. The estuary covers an area of 10,800 km^2 and is 400 km long. Upstream of Quebec City, it features strong convergence and meandering morphology, with the name “Kebec” meaning "where the river narrows". The maximum width at its mouth is 48 km, while widths upstream of Quebec City range from 1 to 2 km.

This macro-tidal estuary (7m maximum tidal range) exhibits tidal amplification up to Île-aux-Coudres during spring tide and up to Saint-François-de-l’Ile-d’Orléans during neap tide [43], followed by a reduction in tidal range upstream, characterizing it as a hypersynchronous estuary. This implies that the forces of convergence in the Upper Estuary exceed those of friction, whereas the reverse holds true in the Fluvial Estuary. Moving upstream, the tide becomes increasingly asymmetrical and asynchronous. The Upper Estuary is nearly vertically homogeneous just downstream of Île d'Orléans, partially mixed between Île-aux-Coudres and Tadoussac, and partially stratified towards Tadoussac ([23], [59]). The Lower Estuary is stratified [59].

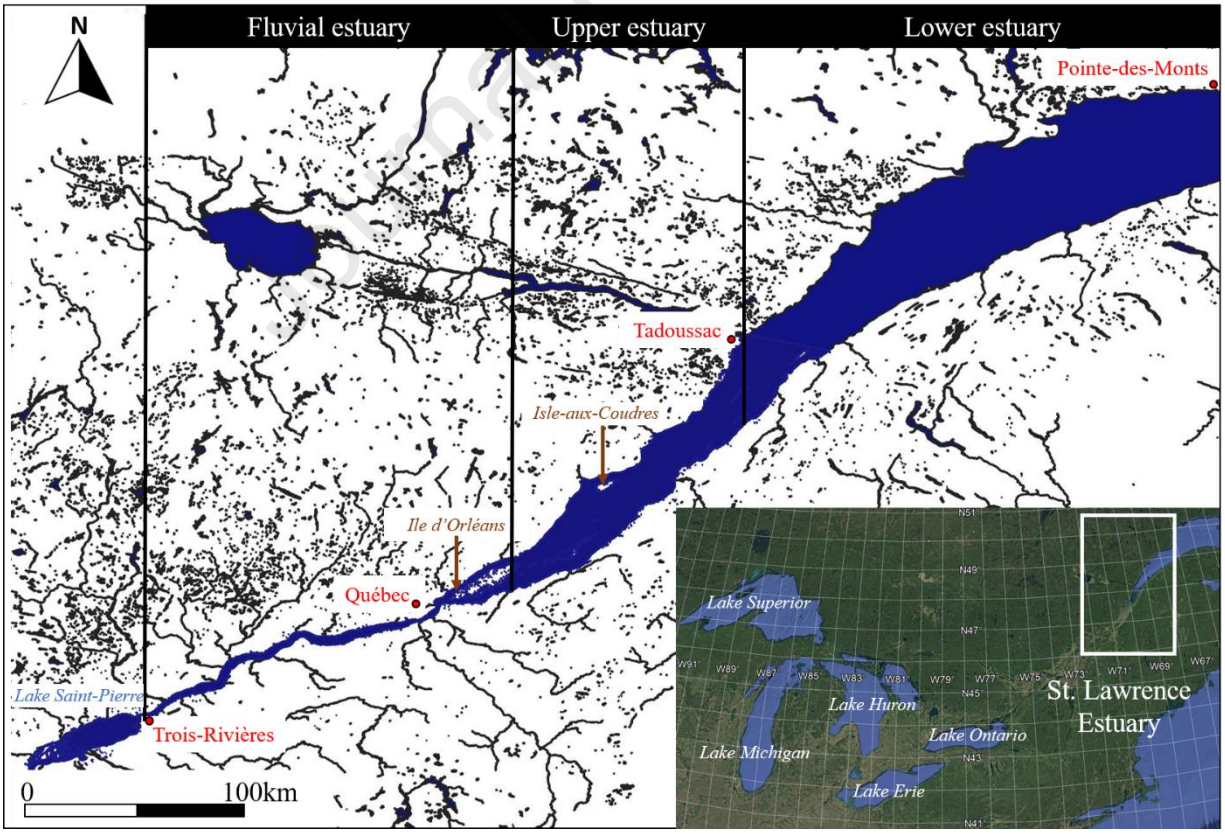

Fig. 1. Map of the St. Lawrence Estuary with location of its three main parts.

The St. Lawrence Fluvial Estuary, the area of interest in this study, is bounded by Lake Saint-Pierre upstream of Trois-Rivières and by the eastern tip of Île d'Orléans, spanning a total length of 180 km. It is characterized by a complex geometry and bathymetry (Fig. 2). This section of the estuary includes the limit of saline intrusion, located just downstream from Île d'Orléans [32], [59], where the turbidity maximum is superimposed [59], [60]. Downstream of Île d'Orléans, three distinct channels of varying depths lead to preferential water circulations. The north channel features depths ranging from -20 and -80 m, gradually increasing from upstream to downstream. The southern channel is discontinuous and shallower (-20 m). The intermediate channel is less marked, intersected by islands that create locally complex hydrodynamics. The bathymetry of the area reveals two significant depressions: one upstream of Île d'Orléans, characterized by strong lateral convergence and a confluence/diffluence zone due to the presence of Île d'Orléans, and the other downstream of Île-aux-Coudres, which is much deeper. This latter depression originates from a meteorite impact nearly 400 million years ago and the Logan seismic fault, which runs along the St. Lawrence and separates the Canadian Shield (north of the river) from the Appalachians (south of the river).

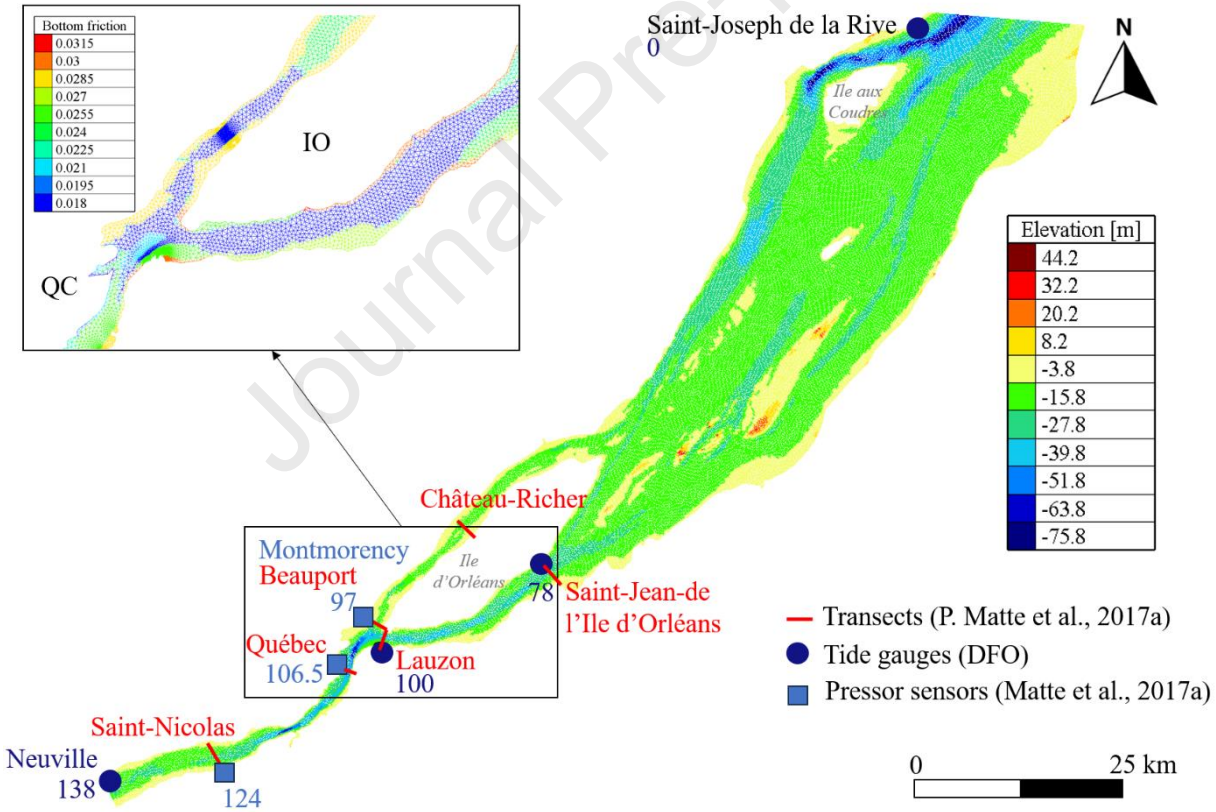

Fig. 2. Mesh of the TELEMAC 3D model of the St. Lawrence Fluvial Estuary with integration of bathymetry and roughness (Matte, Secretan, & Morin, 2017a). Hydrodynamic data localized for the TELEMAC 3D numerical model: tide gauge from DFO (Ministère Pêche Océan), pressure sensors and flows and velocities data from (Matte, Secretan, & Morin, 2017a). QC: Quebec. IO: Ile d'Orléans

The study site corresponds to a macrotidal semi-diurnal asynchronous estuary with tidal ranges of about 6m during spring tides on average. The asymmetry of tides increases from the downstream to the upstream limits, i.e. from Saint-Joseph de la Rive up to Neuville. Based on a nonstationary tidal analysis [42], significant temporal and spatial variability can be observed in the harmonic constituents, mainly associated with their seasonal modulation by river flow and estuarine convergence . The amplitude of diurnal (K_1, O_1) components decreases from the Saint-Joseph de la Rive to Neuville whilst their phases increase in the direction of tide propagation. Similarly, the amplitudes of semidiurnal (M_2, S_2) constituents increase slightly up to Quebec and then decrease. More importantly is the increase of the ratio M_4/M_2 from 0.1 to 0.4 explaining the strong distortion of the tidal signal, and the increase of phase 2 M_2-M_4 lower than 180° associated with the flood-dominant nature of the SLFE [42], [61].

3. Model Setup

3.1. Numerical terrain model

The bathymetric data (Fig. 2) used in this study are sourced from the previous work of Matte et al. (2017a) [56] and incorporate field observations from multiple sources. The deep bathymetric data in the navigation channel were measured by multibeam sonar and are available from the Canadian Hydrographic Service (CHS) website. The data was converted from the chart datum to the Canadian Geodetic Vertical Datum CGVD28. In the shallow water zones, including floodplains and hard structures (ports, marinas and piers), bathymetry was specifically measured in 2012 during a LiDAR campaign [56], with an average resolution of 15 cm.

The roughness data, resulting from previous calibration work by Matte et al. (2017a) [56] are also used in this study. The Manning friction values were first estimated by considering the sediment and vegetation cover of the bed, following the method by Morin et al. (2000a) [62]. Then the final values were obtained through a two-step validation process using a 2DH finite element model. This study benefits from the previously validated friction coefficients, which serve as numerical inputs for the development of the 3D model.

3.2. Hydrodynamic data

Building on the previous study using a 2DH model [43], [56], this study reuses field data on water level, flow velocity and direction, measured during three distinct periods: June 14 to 16, 2009, representing a neap tide; June 22 to 26, 2009, corresponding to a spring tide; and August 19 to 28, 2009, spanning the spring to neap transition. Water level time series with a 3-minute resolution were obtained from DFO tide gauges (http://marees.gc.ca/) near the confluence area during these periods: Lauzon (rkm 100), Saint-Jean-de l'Ile d'Orléans (rkm 78), Neuville (rkm 138) and Saint-Joseph de la Rive (rkm 0) (Fig. 2). These data are supplemented with water level data from pressure sensors from the campaign

208 by Matte et al. (2014) [57], with a time resolution of 15 minutes, at locations including Saint-Nicolas
209 (rkm 124), Québec (rkm 106.5) and Montmorency (rkm 97) (Fig. 2).

210 The velocity data used in this study were obtained from the measurement campaigns [57] along
211 the transversal sections indicated in Fig. 2. These high-resolution data were collected using an RD
212 Instruments Rio Grande Acoustic Doppler Current Profiler (ADCP), at a sampling frequency of 2.5 Hz,
213 a spatial resolution of 50 cm, and a velocity accuracy of ±0.25% (0.25cm/s). This accuracy represents
214 only the instrument's precision, and other potential errors are detailed in the works of Matte et al. (2014)
215 [57]. Flow discharge values were also estimated at Saint-Nicolas, Québec City, Beauport, Lauzon,
216 Château-Richer and Saint-Jean-de-l'Île-d'Orléans [57]. Special attention was given to correct these
217 measurements by accounting for the boat's speed and trajectory, together with the tidal phase. In fact,
218 due to the large widths of the surveyed cross-sections, the data were interpolated both spatially and
219 temporally to reconstruct continuous fields, allowing for direct comparison with instantaneous model
220 outputs. For more details on the measurement and interpolation procedures, readers are referred to [57].

221

222 ## 3.3. Numerical model

223

224 The numerical model of the St. Lawrence Fluvial Estuary is developed using the 3D version of
225 the open-source TELEMAC code (www.opentelemac.org). TELEMAC 3D has been widely used in
226 studies of estuarine hydrodynamics ([27], [63], [64], [65], [66], [67], [68], [69], [70], [71]). TELEMAC
227 is based on the finite element method to solve the Reynolds Averaged Navier-Stokes (RANS) equations
228 on unstructured triangular mesh and the sigma-transformation for the mobile free surface [72]. The
229 RANS equation reads:

230 $$\frac{\partial U}{\partial x}+\frac{\partial V}{\partial y}+\frac{\partial W}{\partial z}=0 \tag{1}$$

231 $$\begin{aligned}
&\frac{\partial U}{\partial t}+U\frac{\partial U}{\partial x}+V\frac{\partial U}{\partial y}+W\frac{\partial U}{\partial z}=-\frac{1}{\rho}\frac{\partial p}{\partial x}+\nu\Delta U+F_x\\
&\frac{\partial V}{\partial t}+U\frac{\partial V}{\partial x}+V\frac{\partial V}{\partial y}+W\frac{\partial V}{\partial z}=-\frac{1}{\rho}\frac{\partial p}{\partial y}+\nu\Delta V+F_y\\
&\frac{\partial W}{\partial t}+U\frac{\partial W}{\partial x}+V\frac{\partial W}{\partial y}+W\frac{\partial W}{\partial z}=-\frac{1}{\rho}\frac{\partial p}{\partial z}-g+\nu\Delta U+F_z
\end{aligned} \tag{2}$$

232 where (U,V,W) are the Reynolds averaged component of velocity (in m/s), ρ (in kg/m^3) the density of
233 water, p (in Pa) the pressure, g (=9.81 m/s^2) the gravitational acceleration, ν (in m^2/s) the effective
234 viscosity, (F_x, F_y, F_z) the external Force component (in m/s^2).

The main advantages of the code are: (i) the use of a 2DH unstructured mesh which can be used for both the 2DH and 3D study, (ii) the sigma-transformation to handle the bed and water moving interfaces, (iii) the performance of the code to run on supercomputer; (iv) the modularity to activate different coupling (sediment transport, temperature and salinity for instance) and turbulence closure options. Here we consider the option with k-ε model in the horizontal and the mixing length model in the vertical similar to other case studies (see [55], [58] for more details).

For this study on the 3D flow dynamics in a macrotidal estuary presenting natural bifurcation with large island, the unstructured aspect of the code enabling high resolution in high gradient region is clearly advantageous to save CPU time. The code enables fine resolution in areas with complex bathymetry and geometry, such as riverbanks and coasts, or underwater canyons, and coarser resolution in areas with low bathymetric.

The numerical methods employed in TELEMAC 3D are extensively detailed by Hervouet [72], thus only briefly outlined here. TELEMAC 3D solves the Navier-Stokes equations for 3D incompressible flows. The hydrostatic version of TELEMAC 3D was used, applying the method of characteristics for the advection scheme, with Thompson boundary conditions imposed [73], [74], and mass lumping applied to the mass matrix of the momentum equation. The linear system is solved by a GMRES method with a diagonal preconditioning.

In this study, the hydrostatic pressure assumption and the Boussinesq approximation is used in order to reduce the computational costs. These assumptions leads to the following simplifications [72]:

$$p = p_{atm} + \rho_0 g(Z_s - z) + \rho_0 g \int_z^{Z_s} \frac{\Delta\rho}{\rho_0} d\varsigma \tag{3}$$

$$\rho = \rho_0 \left[1 - \left(7(T - T_{ref})^2 - 750S \right) 10^{-6} \right] \tag{4}$$

where p_{atm} is the atmospheric pressure, Z_s is the surface elevation, ρ and ρ_0 are the density of fluid and pure water respectively, $\Delta\rho$ the density difference of fluid and pure water. Eq. (4) gives the fluid density as function of temperature, T, (°C) and salinity S (between 0 and 42 g/L) for reference temperature T_{ref}=4°C. Note that in the present application, we fixed water temperature T=18°C and salinity S=0g/L in the whole domain and at all time, given that the area of interest is situated in the freshwater estuary. No atmospheric forcing or coupling was applied in the current model.

The computational domain used is located between Neuville and Saint-Joseph de la Rive. The Manning coefficients were recovered from a 2D model calibrated from detailed level and current measurements [56]. Bathymetric and Manning's coefficient data are interpolated on the 2D mesh, which is a finite element mesh with mixed triangular elements. The 3D model was calibrated by optimizing the mesh resolution both vertically and horizontally, as well as by enhancing the temporal resolution.

Numerical sensitivity was conducted using different meshes varying from 180 to 250m horizontal resolution, with 8, 12, 16, and 20 vertical layers and different time steps from 5 to 10s. The 2D optimal mesh has 36,073 nodes and 69,702 elements. The coarser resolution of the study domain is 250m, and the finer is 25m. The 3D mesh is constructed from the 2D mesh. The vertical grid is divided into 8 horizontal planes using the simple σ transformation. The elementary volumes thus correspond to five-sided prisms. For this study, the time step is fixed to 5s. The upstream and downstream boundary conditions are set by the water levels measured at DFO's stations in Neuville and Saint-Joseph de la Rive during the summer of 2009. To ensure that the model accurately simulates river discharge for the specified water level boundary conditions, a detailed calibration was conducted using current and discharge measurements at multiple cross-sections, a selection of which is presented in Figs. 3 and 4. The riverbanks and bottom are considered as impervious rough and solid boundaries, i.e. non erodible.

3.4. Calibration and validation

To quantify the discrepancies between simulated and observed water levels, flow discharges and velocity, we compute the relative mean absolute error (RMAE), Skill, Nash-Sutcliffe Efficiency (NSE), and root mean square error (RMSE) and bias. They are respectively given by:

$$RMAE = \frac{\frac{1}{n}\sum_n \left||X_{sim} - X_{obs}| - \Delta X_{obs}\right|}{\frac{1}{n}\sum_n |X_{obs}|}$$

$$Skill = 1 - \frac{\sum_n (X_{sim} - X_{obs})^2}{\sum_n (|X_{sim} - \overline{X_{obs}}| + |X_{obs} - \overline{X_{obs}}|)^2}$$

$$NSE = 1 - \frac{\sum_n (X_{obs} - X_{sim})^2}{\sum_n (X_{obs} - \overline{X_{obs}})^2}$$

$$RMSE = \sqrt{\frac{1}{n}\sum_n (X_{sim} - X_{obs})^2}$$

$$Bias = \frac{1}{n}\sum_n (X_{obs} - X_{sim})$$

where X is the considered variable, $\bar{X}$ the time average on n values. The RMAE measures the average absolute error between model predictions and observations, normalized by the mean of the observations. The Skill compares model performance to a reference, with 1 indicating perfect predictions and 0 meaning the model performs no better than the mean of observations. The NSE assesses model efficiency compared to the mean of observations, with an NSE of 1 being perfect and 0 indicating the model matches the average. The RMSE quantifies prediction error, giving greater weight to larger errors,

294 providing a comprehensive accuracy measure. Finally, the bias indicates whether the model
295 systematically overestimates or underestimates the observations, with values close to zero suggesting
296 minimal systematic error.

297

298 4. Results

299 This section aims to compare the results of 1D observed data and 2D numerical hydrodynamic
300 modeling of the SLFE with those obtained from the TELEMAC 3D model. A more detailed analysis is
301 then conducted to better understand the estuary's hydrodynamics, incorporating 3D results that account
302 for fortnightly tidal cycles. The section also includes predictions for parameters that are unmeasured or
303 challenging to measure, such as residual circulation, transverse velocity, and turbulence, to provide a
304 more comprehensive understanding of the estuary's dynamics.

305 4.1. Validation results (1D and 2D)

306

307 4.1.1. Validation with 1D data

308

309 Observed water levels and velocity profiles measured by Matte et al. (2014) [57] in the
310 confluence/diffluence zone of Île d'Orléans are used to validate the model, with a focus on the stations
311 of Quebec City, Beauport, and Lauzon. A hydrodynamic verification is also conducted for the northern
312 (Château-Richer) and southern (Saint-Jean-de-l'Île-d'Orléans) channels to ensure accurate flow
313 representation. Special attention is given to the navigation channel, as it is critical for maritime traffic.
314 By considering the 2DH calibrated values for the bottom friction into the newly developed 3D model,
315 satisfactory results are obtained on the water level, showcasing root mean square error (RMSE) ranging
316 between 15 and 39 cm across the tested stations (Fig. 3). Simulated discharge values agree also well
317 with the measured values, displaying relative mean absolute error (RMAE) ranging between 14% and
318 23% in all stations. However, at Beauport, the outcomes are comparatively less satisfactory due to the
319 misrepresented peak flow at 4 p.m., with an RMAE of 40% (Fig. 4). A similar error was obtained by
320 Matte (2014) [24] with a 2DH model, pointing to uncertainties in the space-time interpolation of the
321 transect data at this location due to a larger temporal gap in the data around peak ebb flow.

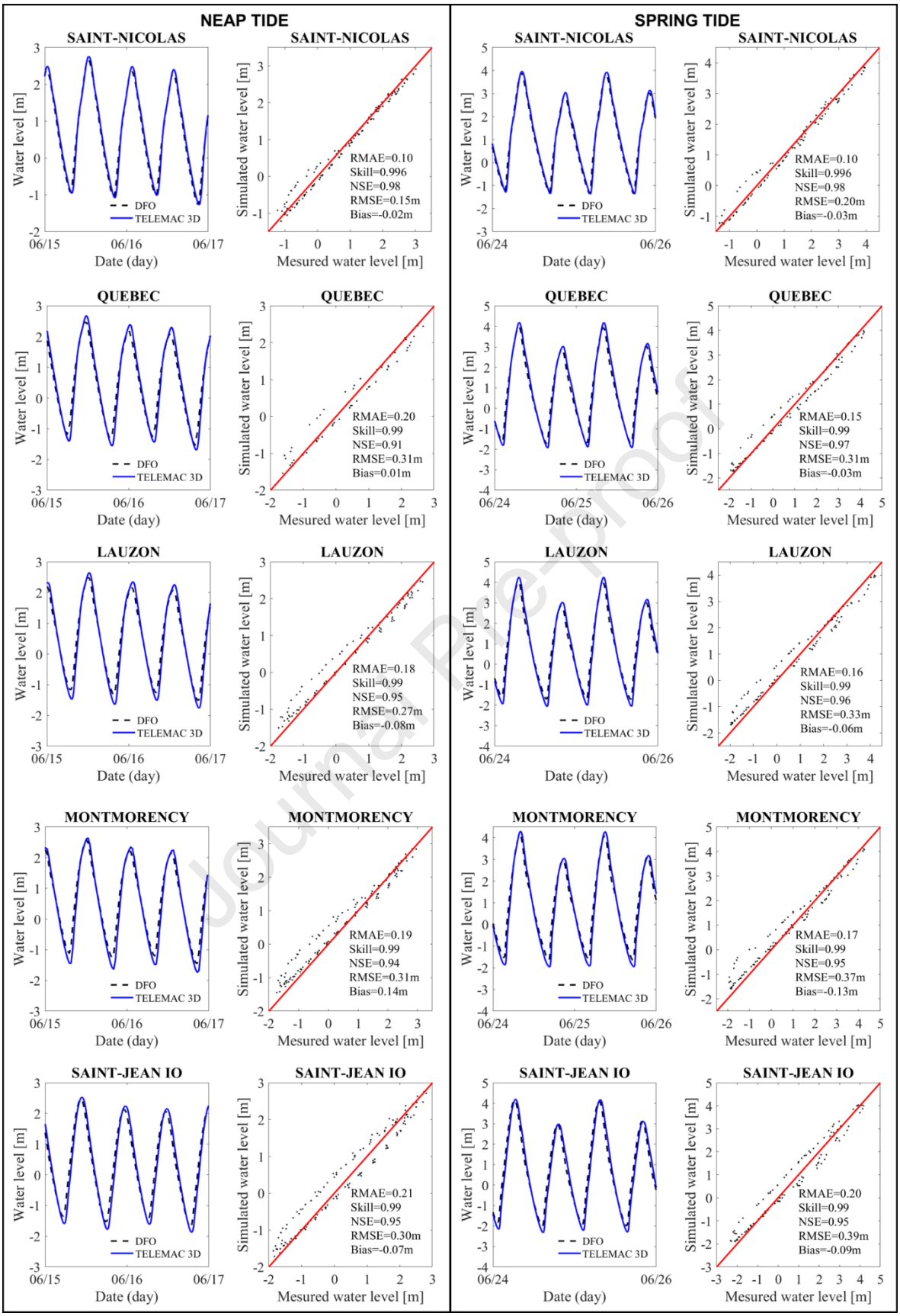

Fig. 3. Simulated water elevations from TELEMAC 3D (blue line) and measured water elevations from the Department of Fisheries and Oceans (DFO) (black dotted line) at tide gauges and pressure sensors during neap and spring tide. Scatterplot of field and calculated water level data with errors: RMAE, Skill, NSE, RMSE and bias.

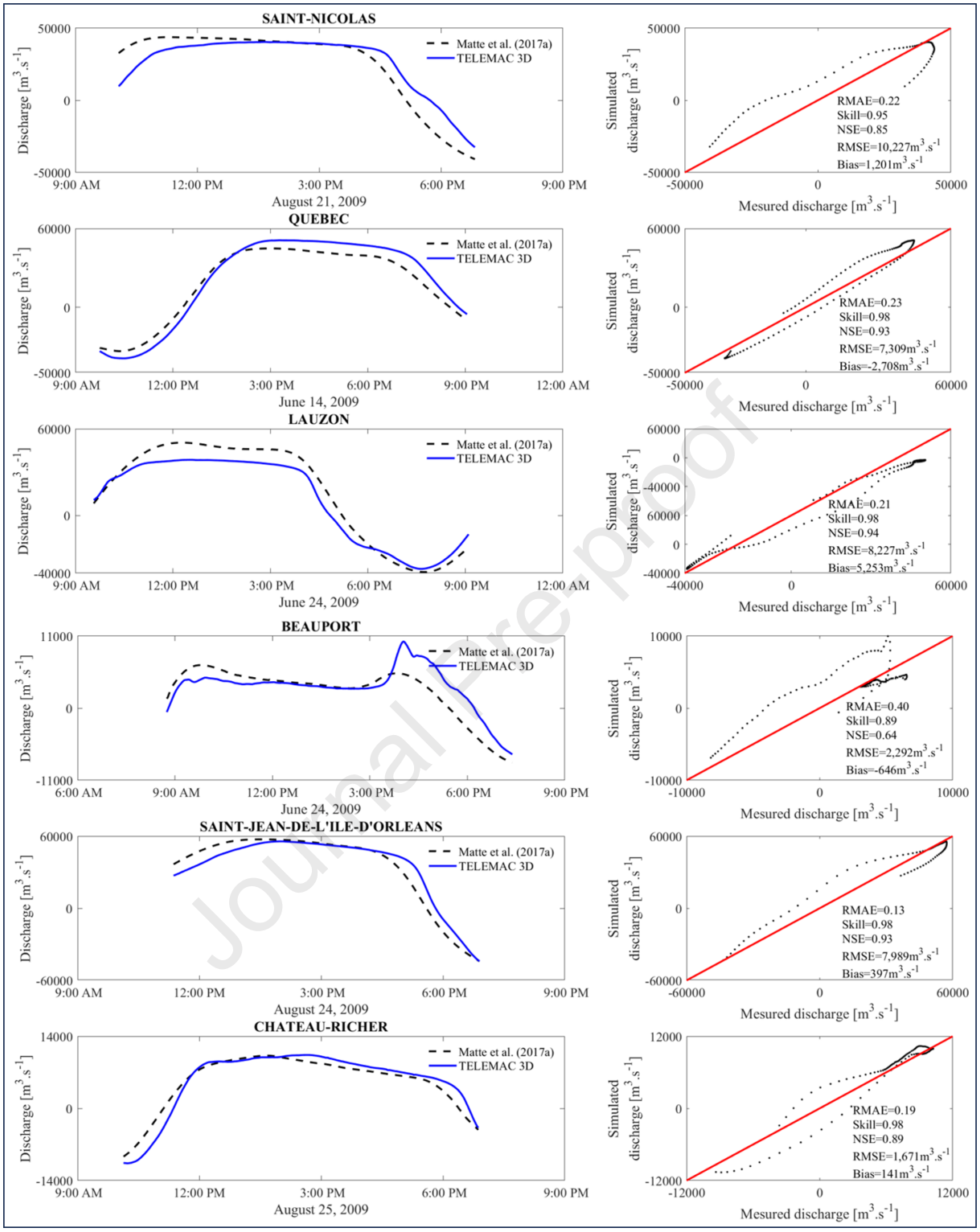

Fig. 4. Simulated discharges from TELEMAC 3D (blue line) and measured discharges (black dotted line) at different transects of the St. Lawrence River estuary (Matte et al., 2017a). Scatterplot of field and calculated discharges data with errors: RMAE, Skill, NSE, RMSE and bias.

4.1.2. Comparison with 2D data

This section presents a comparative analysis between the newly developed 3D model using TELEMAC and the previous 2DH model developed by Matte (2014) [24] using the H2D2 software (https://gitlab.com/h2d2). In order to make this comparison, the 3D results were integrated on the vertical. Both models apply the finite element method based on unstructured triangular meshes, but the former is based on T3 elements (Triangle with 3 nodes) in horizontal and a non-conservative form of the flow equations while the latter considers T6 elements (Triangle with 6 nodes) and a conservative form of the shallow water equations.

Even if it may seem biased to compare the results from the 2D simulations with those from the 3D model, this comparison is justified in terms of velocity fields in areas where the flow has not been measured. This qualitative comparison is proposed in Fig. 5 at the Y-junction close to the Île d'Orléans showing recirculation patterns during spring tides on June 24, 2009. Overall, the 3D model replicates fairly well the recirculation phenomena at the Île d'Orléans junction. From a quantitative aspect, we note that the depth averaging numerical procedure of the 3D model gives velocities systematically lower than the 2DH model by Matte. This discrepancy, observed for different tested vertical resolution (not shown), may be due to the tridimensionality of the flow in the junction zone during a tidal cycle.

During the slack of high water (7:06 a.m.), the main flow is directed to south-west from the two arms of the St. Lawrence fluvial estuary at Île d'Orléans. Fig. 5 presents similar results on velocity magnitude and direction between the 2DH previous simulations by Matte et al. (2017b) [43] and the newly developed 3D model mimicking the depth integrated results.

At HW+1, one hour after the slack of high water, tidal currents continue to flow upstream (to south-west) in the deep channels, and the ebb current initiates at the north riverbank near Beauport. The superposition of the ebb and the remaining flood currents form a second recirculation cell at the corner of the Île d'Orléans. At HW+2, two hours after the high water, ebb current (directed to north-east) is completely developed in the junction zone: the main stream is divided in two branches but is mostly deviated to the southern channel of the Île d'Orléans. At LW-1, i.e. the end of ebb tide, velocities have reached their maximum value of 2.3 m/s as the result of a non-linear combination of river flow and ebb tidal current. The flow analysis shows a strong deflection of the river flow to the southern channel and two detachment zones, the first is located on the other side of Quebec City (close to Lauzon tidal station), the other in the south corner of the Île d'Orléans. The latter flow detachment at the corner of island is very similar to what is observed during flow separation at a junction. The two face to face recirculation zones create a zone of maximum flow speed and may explain the high value that the model predicts.

At the slack of low water (LW, 3:24 p.m.), the currents progressively slow down and change suddenly direction in the southern branch as the tide rises (flood). The rapid reversal of current direction

from ebb tide to flood tide is explained by the strong tidal asymmetry which is characterized by a water level falling period of 8h and a rising period of 4h during the flood. At LW+1, one hour after low water, current reversal happens in the south branch, but the flow accelerates to maximum value (nearly 1 m/s) toward north-east direction in the north branch.

Two hours after low water, LW+2, the flood current occupies the full section of the south channel, turns around the south corner of the Île d'Orléans. In the north channel, this redirected current encounters the flood current which flows in opposite direction and gives rise to an intense shearing zone. The clockwise circulation of flow around the island from south to north branches of the Y-junction vanishes with time. At HW-1 (or LW+3), the flood currents are fully developed in the entire region of the Y-junction meaning that the tidal regime dominates the fluvial regime completely. Symmetric to the case of well-developed ebb current at LW-1, the well-developed flood current at HW-1 presents flow velocity faster in the south channel (1.5 m/s) than in the north channel (0.5m/s).

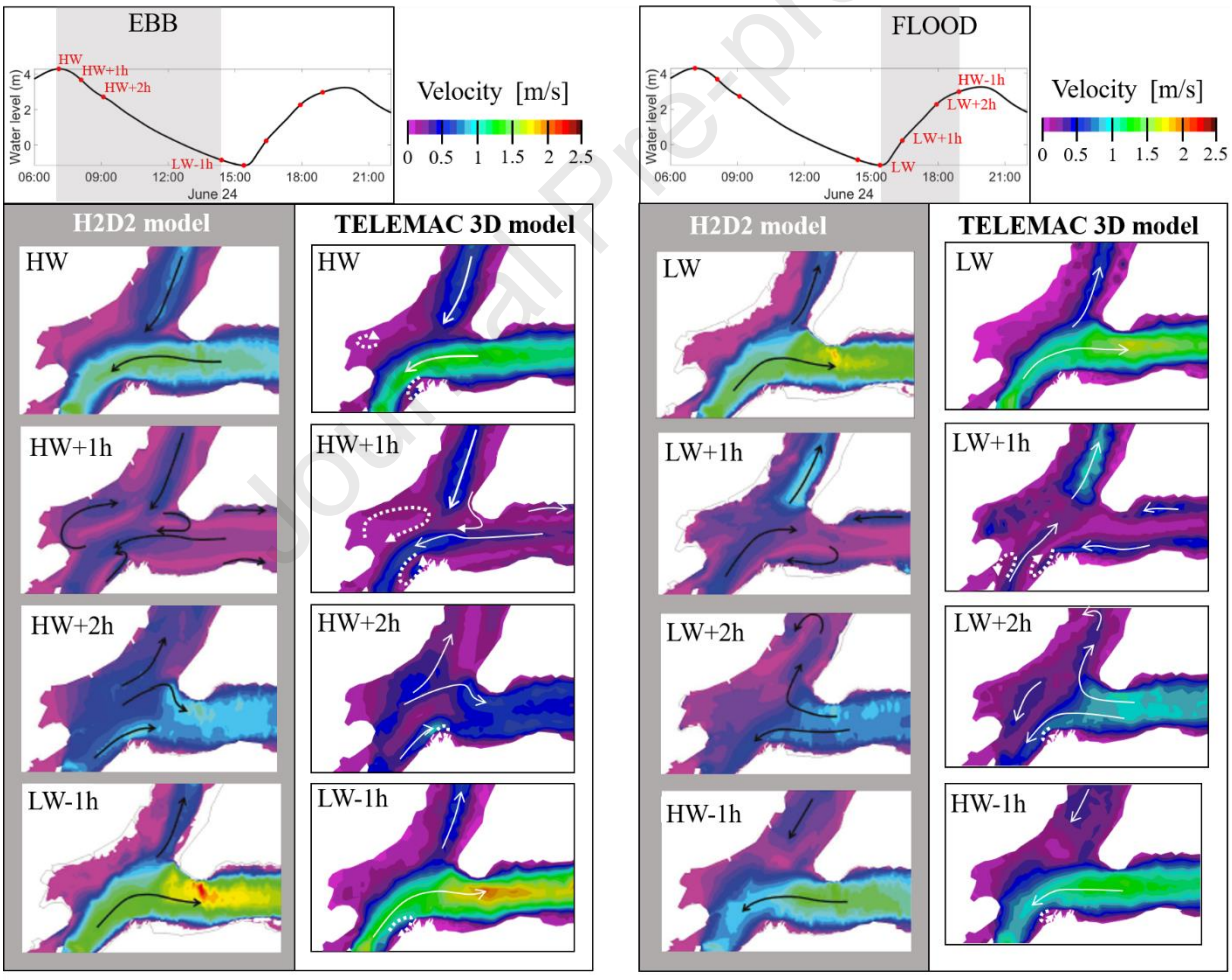

Fig. 5. Comparison of ebb (HW, HW+1h, HW+2h and LW-1h) and flood (LW, LW+1h, LW+2h and HW-1h) tide velocity maps from results simulated with the H2D2 model (adapted from Matte et al., 2017b) (left, grey background side) and TELEMAC 3D (right side) at the Île d'Orléans junction at different tidal stages. Solid arrows indicate current and dashed arrows indicate 3D structures. The tidal signal for June 24, 2009 (spring tide) is shown at the top of the figure (results from TELEMAC 3D modeling). HW corresponds to high tide and LW to low tide.

The depth integrated 3D results using 8 vertical layers are in fair agreement with the original 2DH results based on H2D2 code [43]. The mixed tidal and fluvial dynamics predicted by the 3D and the 2DH codes present very similar flow patterns along a tidal period. The phase difference between vertical (water level) and horizontal (current) tides are fairly close. Moreover, the mixing of the flood current with the opposing redirected current occurs at the same place and time in both the H2D2 results and the depth-averaged data derived from the new 3D model: in the Beauport zone (HW+1) and in the north channel (LW+2). Finaly the value and the time-space location of maximum velocity are very consistent between the two models.

These results, including the 1D calibration (Figs. 3 and 4) and the 2D flow velocity comparisons at different times, show that the 3D model accurately captures the hydrodynamics in the three-branch zone near Quebec City. The next section is thus devoted to the three-dimensional description of the flow dynamics.

4.2. 3D results

4.2.1. Transversal circulation (2D vertical)

In the presence of a confluence marked by the Île d'Orléans, it is easy to draw an analogy with a bridge pier and a meandering river [75]. Similar to this example, the flow stop point at the upstream end of Île d'Orléans would lead to flow bifurcation and to the formation of helical currents on either side of the island. Naturally, these secondary currents downstream could be amplified during ebb tide periods or conversely attenuated during flood tide periods. Similarly, the coexistence of very deep (-30m) and less deep (-15m) zones, or the presence of strong bathymetric gradients in a relatively narrow section, could also generate significant heterogeneities in velocity distributions. A cross-sectional analysis of currents enabled by 3D modeling helps to highlight these characteristics.

The 3D model exhibits a notable advantage over previous models by efficiently capturing the lateral hydrodynamics within the St. Lawrence fluvial estuary. This attribute holds significance for examination, particularly concerning the presence of recirculations within the junction zone, warranting detailed investigation. In this section, the surface normal velocities of the Lauzon transect are shown during both neap and spring tides (Fig. 6a and Fig. 6b).

The analysis of recirculation at Lauzon provides additional information than the 2D horizontal. Here, the complexity of the flow dynamics in the tidal junction zone is particularly highlighted on the vertical and transverse velocity profiles. Fig. 6 presents a significant vertical component along the bathymetry gradient and an important difference in the lateral flow magnitude and direction (further discussion is provided in section 5.2). The direction of lateral velocity vectors can be attributed to the tidal influence itself. Circulation is directed towards the south bank during flood period (with a greater

420 influence of tide) but towards the north bank during ebb period, when the river's discharge combines
421 with the tidal discharge. Examination of surface normal velocities indicates maximum speeds of 1.5 m/s
422 during spring tide compared to 1.3 m/s during neap tide at low water minus one hour (LW-1). Similarly,
423 minimum velocities (or, equivalently, maximum flood velocities) are stronger during spring tide (-1.2
424 m/s) than during the neap tide (-0.7 m/s).

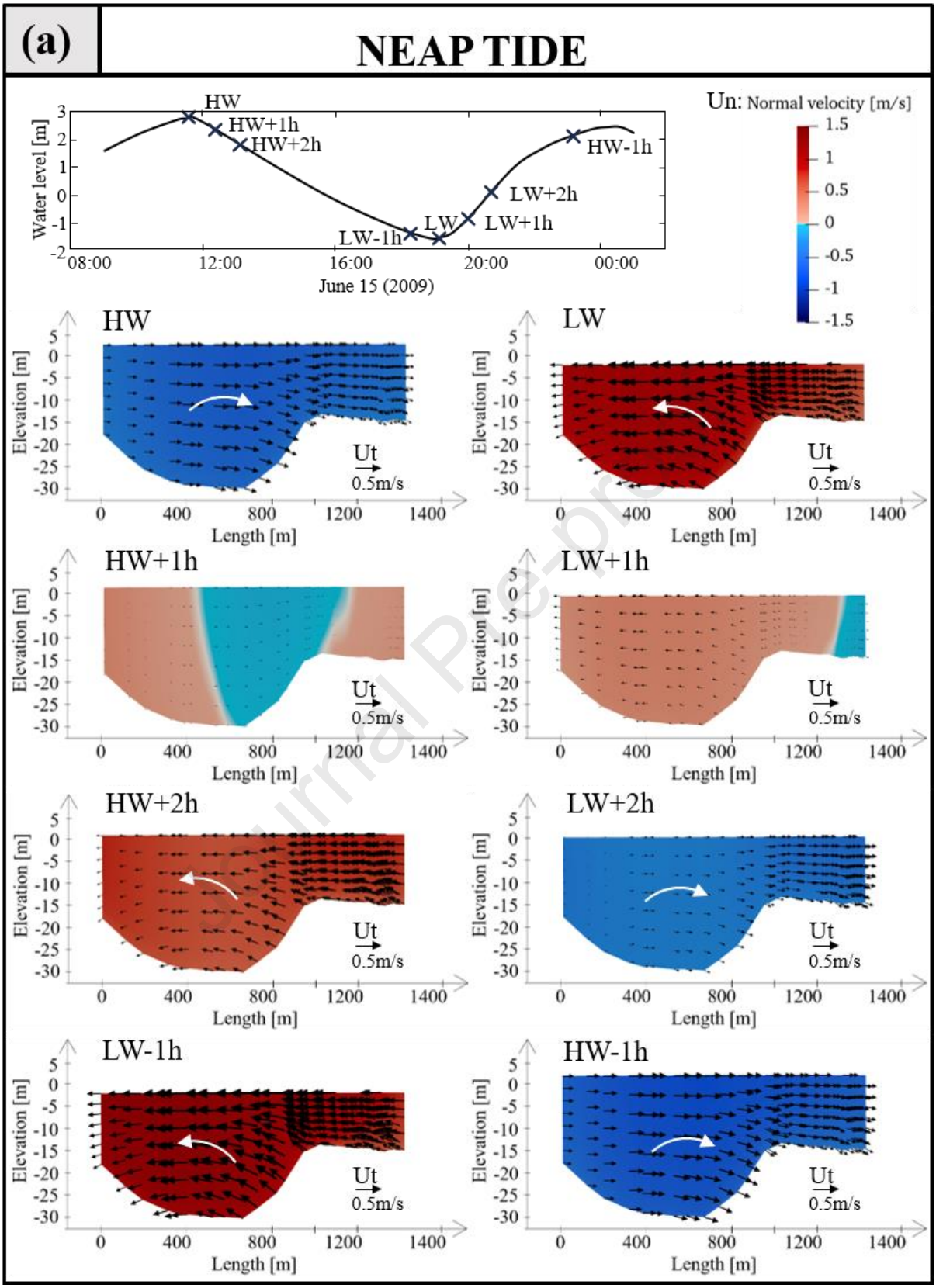
(a)
NEAP TIDE
Un: Normal velocity [m/s]
1.5
1
0.5
0
-0.5
-1
-1.5
Water level [m]
HW
HW+1h
HW+2h
HW-1h
LW+2h
LW
LW+1h
LW-1h
08:00
12:00
16:00
20:00
00:00
June 15 (2009)
HW
LW
HW+1h
LW+1h
HW+2h
LW+2h
LW-1h
HW-1h
Elevation [m]
Length [m]
Ut
0.5m/s

425

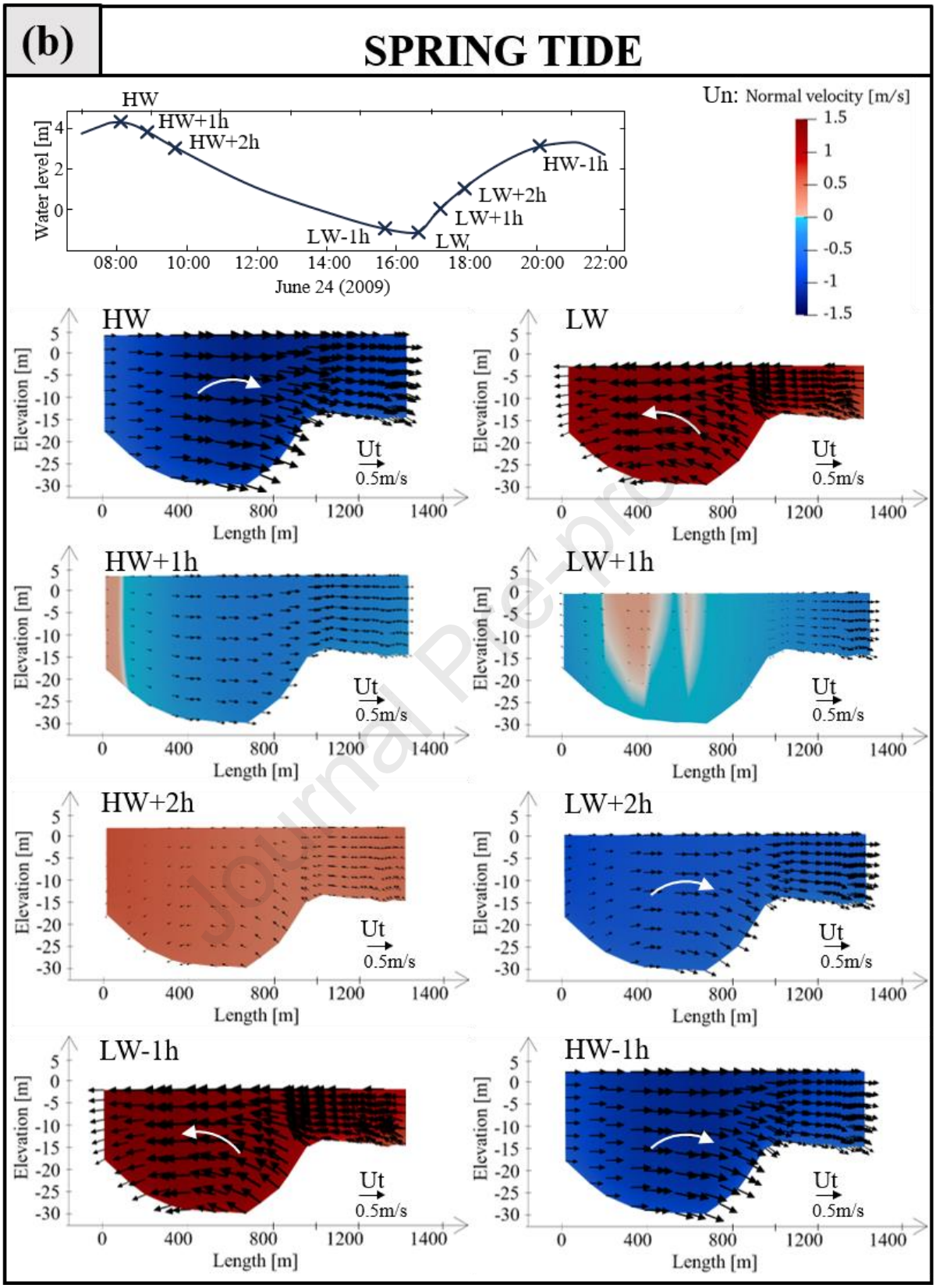

426

427 *Fig. 6. Graph illustrating the velocity evolution at the Lauzon cross-section (a) during neap tide (b) during spring tide. The*
428 *velocity along the channel (normal velocity Un) is represented with the color bar, with positive values referenced in the*
429 *downstream direction of the river (results from TELEMAC 3D modeling). Lateral channel velocities (Ut-Uz) are represented*

by black arrows and the white arrows represent the lateral global direction (results from TELEMAC 3D modeling). HW refers to high water, and LW refers to low water.

The analysis of the vertical component of velocity is particularly crucial in the junction zone, which behaves like a confluence or a divergence zone depending on the tidal phase as depicted in Fig. 6. The coexistence of a deep main channel (26m) and shallow banks (15m) leads to heterogeneity in current velocity distribution. Current reversal occurs earlier along the banks and later in the main channel. This can be explained by three distinct phenomena: (i) the confinement of flow in the main channel, leading to a more uniform flow, may result in a longer response time of the current to tide changes compared to the banks, (ii) the friction affecting the bank plateau results in lower velocities and thus a quicker response and (iii) the remaining backflows along the convex banks (Fig. 5) at the onset of ebb tide (HW+1) and flood tide (LW+1), contributing to the observed current reversal patterns.

These transition states (HW+1 and LW+1) correspond to the reversal of the tide and result in opposing currents, in contrast to the fully developed ebb and flood currents (HW-1 and LW-1). A hysteresis effect can also be observed, with the flow persisting in the same direction beyond the change in tidal direction. This is particularly noticeable at HW+1 (during neap tide), where despite the start of the ebb tide, currents continue in the direction of the flood tide due to the water already introduced into the estuary, creating a time lag between the tide and the flow. A one-hour phase shift is observed between high tide and current slack, where the current is almost zero, occurring at HW+1 as mentioned by Matte, Secretan, & Morin, 2019 [76]. A temporal evolution of ebb and flood currents is also asymmetrical between neap tide and spring tide periods. Indeed, ebb currents during neap tide reverse more rapidly than those during spring tide, and vice versa for the flood period (Fig. 6). This asymmetry is visible at the junction in the simulated periods. At Lauzon, the time lag between high water slack (HWS) and HW increases during spring tides compared to neap tides, averaging from 66 to 77 minutes. Conversely, the lag between LW and low water slack (LWS) is reduced during spring tides, decreasing from 86 to 42 minutes. The same orders of magnitude can be observed for the 2D model [43].

4.2.2. Turbulence energy

The turbulent kinetic energy (TKE) represents the energy contained in the turbulent eddies and flows of a fluid and is defined as:

$$k = \frac{1}{2}\left(\overline{u'^2} + \overline{v'^2} + \overline{\omega'^2}\right) \quad (5)$$

where k is the turbulent energy (in J/kg) and u', v', ω' are the fluctuation velocity components (m/s).

In this 3D study, the effects of turbulence are modeled by a variable turbulent viscosity derived from a standard k-ε model in the horizontal plane and a mixing length model in the vertical plane. The

latter is specifically used to account for the vertical/horizontal inherent anisotropy of natural free surface flow, which are mainly characterized by vertical length scale smaller than horizontal length scale. Moreover, this choice is consistent with future perspective of the proposed 3D development aiming to include density stratification of estuarine water under thermal or salinity gradient.

In the context of velocity differences between the deep main channel and the shallow bank plateau, the significant shear stress generated at the interface due to varying flow speeds (Fig. 6) is a primary source of turbulence (Fig. 7). In the deep main channel, where flow is more uniform, shear stress and turbulence are relatively lower. In contrast, near the shallow bank plateau, the flow experiences a very steep velocity gradient and develops higher shear stress and more turbulence. This enhanced turbulence at the shallow-water interface facilitates mixing between sigma-layers and plays a key role in current inversion phenomena. Turbulence attenuates the difference between flow areas, especially between the shallow bank and the deep channel. It affects how long and strong the current inversion lasts by mixing the water masses. This mixing reduces the strong velocity gradient between the shallow and deep areas, influencing the duration and intensity of the inversion.

Predicting turbulence parameters in multi-layered or compound channels is challenging due to the lateral exchange of momentum in the shear layer, which forms between the faster water in the main channel and the slower water in the floodplain [77]. As a result, shear stress gradient impacts both turbulence energy distribution and current reversal dynamics specific to tidal junction, emphasizing the importance of turbulence in SLFE's hydrodynamics.

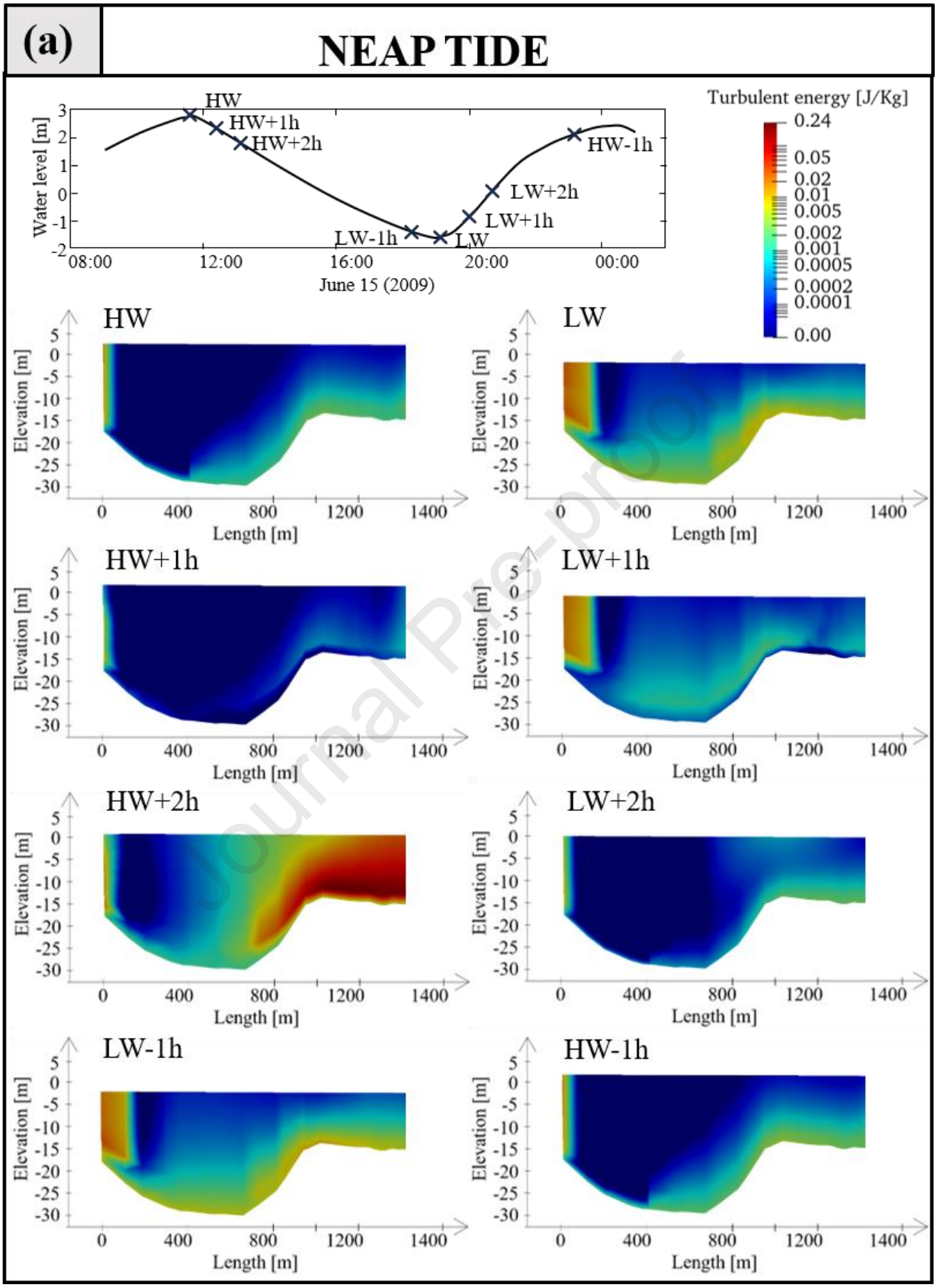

482

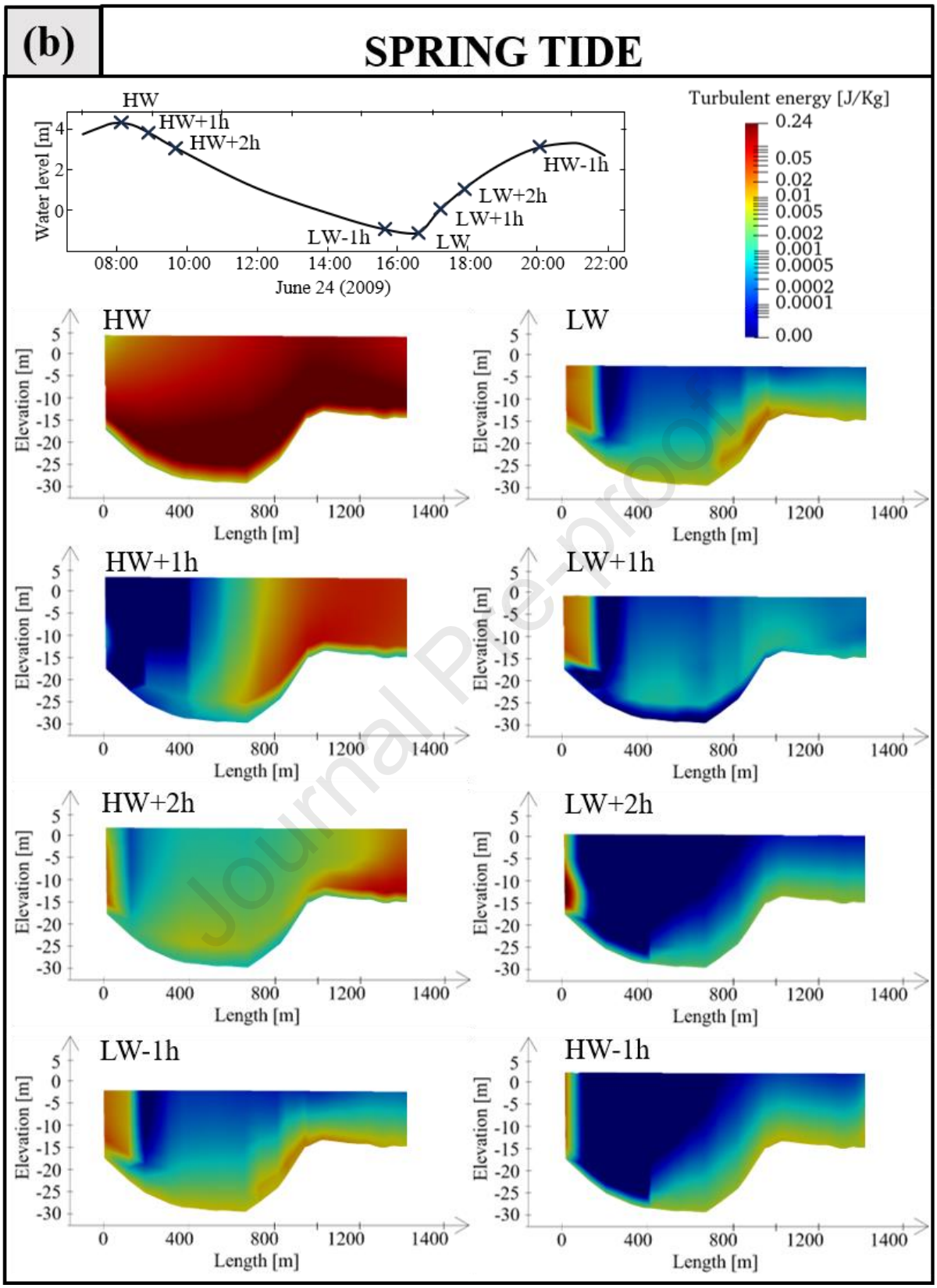

483

484 *Fig. 7. Graph showing the evolution of TKE at the Lauzon cross-section (results from TELEMAC 3D modeling) (a) during neap*
485 *tide and (b) spring tide. HW corresponds to high water and LW to low water. Cross-section orientation: North bank on the left,*
486 *south bank on the right.*

Fig. 7 presents the results on turbulent kinetic energy (TKE) distribution across the Lauzon section and over the tidal phase. In general, the 3D model predicts higher TKE values in the bottom region, with a TKE hotspot near the corner of the plateau's right (convex) bank during tidal slack (LW, HW). At HW+1 (spring tide: Fig. 7b) and HW+2 (neap tide: Fig. 7a) the cross section presents two very different regions with high TKE values at the right (south) bank. At the initiation of ebb period, the ebb current is not completely developed across the section and is localized in the near bank region whilst the previous flood current continues to flow in the central zone, i.e. in the deep channel. The coexistence of downstream (bank) and upstream (channel) flow velocities generates an intense shearing and recirculation zone which explain the high TKE region at the right and convex bank. Fig. 7a (neap tide) shows that the TKE distribution is quasi-homogeneous at LW-1 and HW-1, particularly in the transversal flow of velocities (Fig. 6a). The TKE field is more homogeneous between LW+2 until HW+1, which reflects a more stable period for turbulence distribution.

The TKE results have shown that the zone and intensity of turbulence vary both spatially and temporally, depending on the tidal phase and the bathymetry. Combined with the velocity fields results (sections 4.1.2 and 4.2.1), the analysis of TKE deepens the understanding of hydrodynamic processes during tidal current reversal. Furthermore, these quantities may play a fundamental role in the mixing of temperature and salinity, though this aspect is beyond the scope of this paper.

5. Discussion

5.1. Interpolated measurements versus 3D numerical data

The St. Lawrence fluvial estuary is a highly complex site characterized by strong bathymetric gradients, tides, intense currents, and the presence of the tidal junction, making velocity measurements particularly challenging. Due to these particularities, ADCP velocity measurements are conducted by boat along repeated cross-sectional tracks. However, this method has well-known limitations, such as the time required to complete measurements along a given transect and the need to follow specific measurement trajectories. These limitations are particularly important at this study site due to the wide cross-sections (>1 km) and the highly transient vertical velocity gradients (section 4.2.1) and turbulence (section 4.2.2). Therefore, it is mandatory to use spatiotemporal interpolation methods, such as those applied in [57], to accurately compare field measurements with synoptic model outputs at any given time. While these methods are effective in most cases, numerical models can offer valuable supplementary information. Space-time interpolation methods are suitable when currents are well developed and when there is a minimal variation in water levels during data collection. For instance, at Lauzon, at 15:44 (approximately LW-1, Fig. 8a), Fig. 8b and Fig. 8c show a velocity difference of 12% (relative RMAE) on the Lauzon transect between the interpolated data and the TELEMAC 3D model.

However, these interpolations are more challenging when tidal currents are in a transient phase (section 4.1.2), with local velocities moving in opposite directions, particularly at the interface between the deep channel and shallow plateau (section 4.2.1) characterized by sharp contrasts in velocity magnitude and direction. In this case, at Lauzon, a better correspondence between the experimental (space-time interpolated) data at 16:56 and the numerical (instantaneous) model is obtained by identifying the time t that minimizes the deviation between the observations and the numerical predictions. We obtain a fair agreement for t=17:06 (Fig. 8a, 8d, 8e). The difference between these two velocity fields is 67% (relative RMAE), mainly due to discrepancies in the location of the current shear zone at the deep channel/shallow plateau interface.

Field measurements with higher temporal resolution (e.g. using fixed ADCP, or repeated ADCP transects with two boats moving in opposite directions) would improve the spatiotemporal interpolation of rapid, localized current variations, particularly in areas with strong velocity gradients, which otherwise limits the validation of 3D numerical models. Concurrently, 3D numerical results with finer spatial resolution can complement these measurements, offering a more detailed perspective on the complex dynamics at the tidal junction and guiding data interpolation in regions with strong velocity gradients.

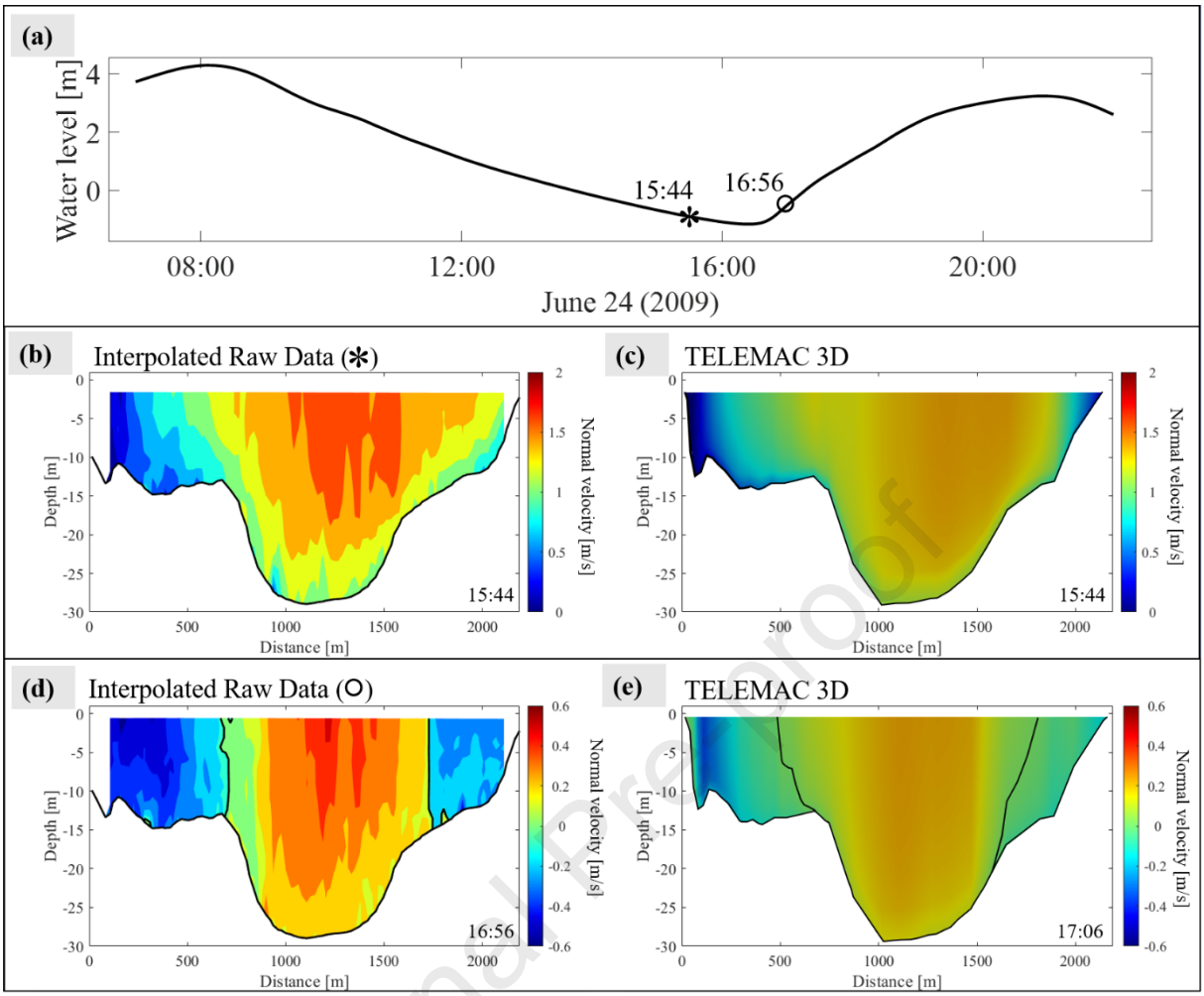

Fig. 8. (a) Water level at Lauzon (June 24, 2009). (b) Spatiotemporally interpolated velocities at 15:44 (June 24, 2009) at Lauzon using the synopticity method of Matte et al. (2014). (c) Instantaneous velocities calculated with TELEMAC 3D at 15:44 at Lauzon (d) Spatiotemporally interpolated velocities at 16:56 (June 24, 2009) at Lauzon using the synopticity method of Matte et al. (2014). (e) Instantaneous velocities calculated with TELEMAC 3D at 17:06 at Lauzon. The thick black line shows the zero velocity contour line and the river bed.

5.2. Dynamics of the Île d'Orléans tidal junction

This section aims to summarize the previous results by cross-referencing the velocity data on the Lauzon transect (Fig. 6) with those from the TKE (Fig. 7), while integrating the timing of the water level signal and geometry influences at the tidal junction (Fig. 5). These cross-references provide a better understanding of the hydrodynamic processes observed, particularly in relation to current reversals and shear phenomena, as previously mentioned in the analysis of high-turbulence zones. Fig. 9 shows typical 3D results, demonstrating the importance of considering a 3D model for this area in transitional state (HW+1), particularly for future studies on salinity or dispersion of pollutants.

At HW-1, the current is fully developed with relatively homogeneous normal velocities over the entire section. The normal velocity amplitude is -0.7m/s during neap tide (Fig. 6a) and -1.5m/s during spring tide (Fig. 6b). Lateral currents in the south channel are strong and clockwise (Fig. 6), with a high TKE region located on the south bank (Fig. 7). This orientation of the lateral currents can be largely

554 explained by the geometry of the site, involving: (i) the orientation of the inflow towards the south bank
555 by the slightly curved tip of the Île d'Orléans; (ii) the significant difference in depth between the main
556 channel and the south bank (Fig. 5). Then, when the water level reaches its maximum (HW), normal
557 and lateral velocities in the south arm decrease overall. Turbulence is virtually homogeneous laterally,
558 and is greatest at the bottom of the channel and bank (frictional forces), and highest at the junction
559 between the main channel and the plateau on the south bank of the south arm, due to the sudden change
560 in bathymetry (Fig. 7 and Fig. 8). Turbulence is greater in spring tide than in neap tide, due to the greater
561 influence of the tide causing stronger currents.

562 From HW, normal velocities on the south bank of the south arm begin to fall to zero, until the
563 current becomes opposed to the main channel current (Fig. 6). The width and depth of the main channel
564 create a confining effect, making the flow more uniform and concentrated than on the banks. This
565 implies a slower response time to changes in tidal direction, due to greater hysteresis in the channel than
566 on the banks. This opposition persists and becomes more pronounced at HW+1. This is the transition
567 phase of the ebb tide currents, where recirculation phenomena are present due to the weaker tidal
568 influence compared to that of the river. Lateral velocities are almost null at HW+1 in neap tide (Fig. 6a)
569 and almost null between HW+1 and HW+2 in spring tide (Fig. 6b), underlining a faster transition time
570 for ebb tide currents in neap tide than in spring tide. The opposing currents between the bank and the
571 deep channel at HW+2 (neap tide Fig. 6a) and HW+1 (spring tide Fig. 6b, Fig. 9b, Fig. 9c) generate
572 high shear forces and turbulence on the south bank of the south channel (Fig. 7). These high-shear zones
573 are described by dashed arrows in Fig. 5 showing complex 3D flow patterns. Fig. 9a illustrates more
574 specifically the vortex area close to Lévis (LV) at HW+1. Vertical opposing currents are highlighted in
575 Fig. 9d, showcasing 3D shear forces and turbulence due to the z-component velocity. At HW+2, the
576 current begins to flow in a more downstream direction. The orientation of lateral velocities reverses
577 counter-clockwise, as the downstream flow is deflected mainly by the geometry of: 1. the tip of Île
578 d'Orléans, which appears to be a concave bank; 2. the overhang of the south bank at the entrance to the
579 south arm (Fig. 7).

580 After this, the main current continues to impose itself downstream until it reaches a fully
581 developed current state, with maximum normal and lateral velocities in the south arm at LW-1 (Fig. 6).
582 Thereafter, velocities continue to decrease while maintaining a downstream (normal) and counter-
583 clockwise (lateral) flow direction (Fig. 6). At low tide (LW), velocities generally decrease again, with
584 lower velocities at bank level. As at high tide (HW), turbulence is high at the bottom (frictional forces)
585 and maximum at the junction between the main channel and the plateau on the south bank of the north
586 arm, due to the sudden change in bathymetry and the observed difference in velocity (Fig 6. and Fig. 7).

587 At LW+1 (beginning of the flood), a second transition period occurs. River currents remain
588 dominant, but the influence of the rising tide increases. These favor return currents in the south arm,

589 with increased turbulence (Fig. 8) accentuated by the geometry of: 1. the tip of the Île d'Orléans, which
590 blocks and redirects the flow in the manner of a convex bank; 2. the south shore, which favors the
591 creation of eddies along the banks (Fig. 5). The influence of the tide increases in the south arm, and
592 currents are once again directed upstream. Part of the flow is redirected towards the north arm where
593 the ebb flow is dominant. Then the flow is redirected upstream as the tide also rises in the north arm
594 (LW+2), although with a phase delay compared to the south arm. Eventually, the currents stabilize,
595 returning to the developed current state at HW-1.

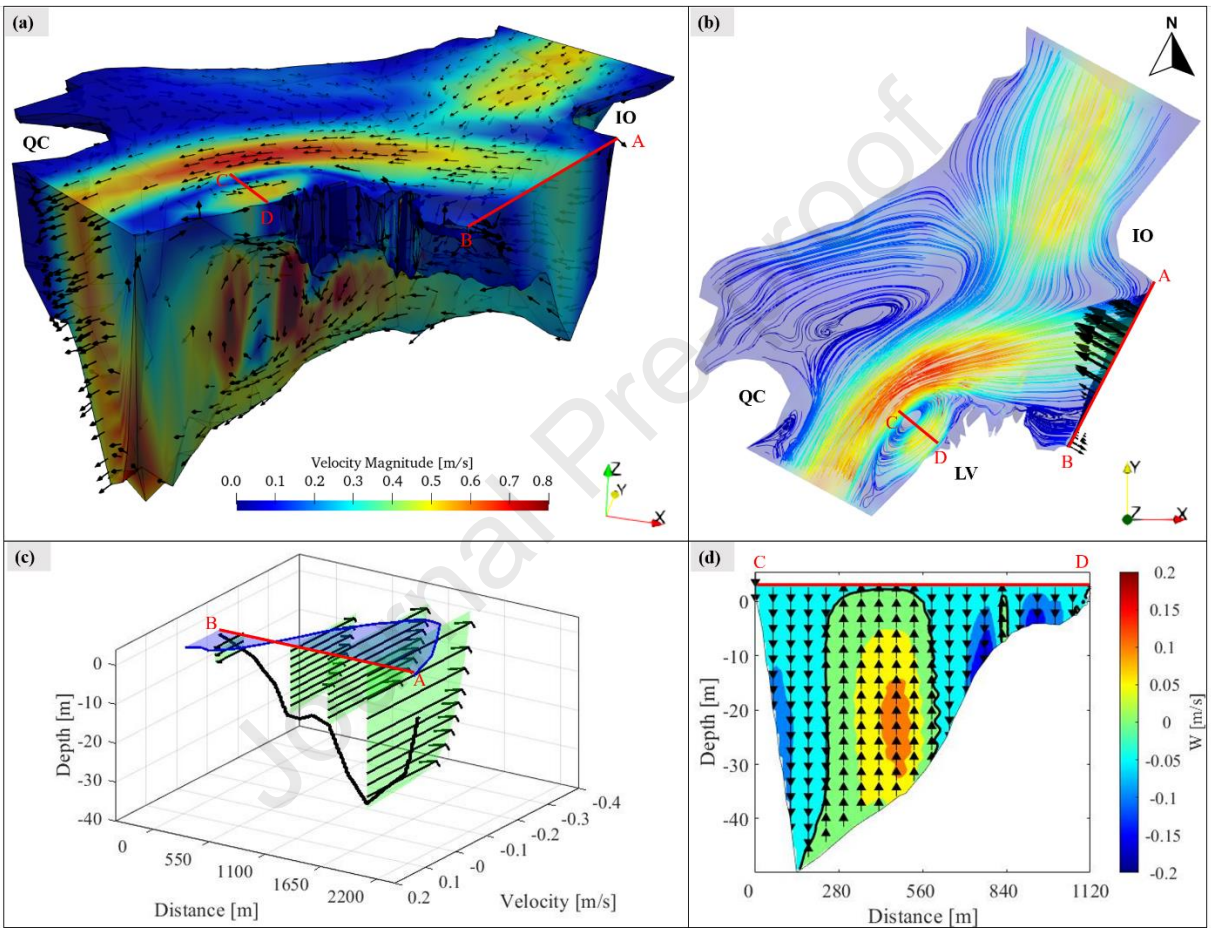

596

597 *Fig. 9. (a) 3D visualization of the hydrodynamics at the diffluence/confluence zone of the Île d'Orléans junction at high tide*
598 *and an hour (HW+1). (b) Top view of the 3D representation showing stream lines, vortices and rip currents. (d) Section AB*
599 *located at the Lauzon transect shows depth-integrated mean velocity (blue) with vertical velocity profiles (green). The thick*
600 *black line represents the bottom. (d) Section CD shows the cross-section of the vortex, highlighting the vertical velocity. The*
601 *thick black line shows the zero velocity contour line.*

602 6. Conclusion and perspectives

603 A 3D numerical model was developed to investigate the hydrodynamics of the St. Lawrence
604 fluvial estuary, aiming to deepen our understanding of this complex environment. The 3D model is
605 obtained from a 2DH model while retaining the same friction coefficient values. Verification of the 3D
606 model was carried out using 1D, 2D and 3D data. Utilizing the TELEMAC 3D software, the model

607 reveals essential insights into the vertical, horizontal, and temporal evolutions in the SLFE's dynamics.
608 Calibration was performed using field data from neap and spring tide periods, with the model
609 demonstrating generally satisfactory consistency between observed and simulated water elevation,
610 discharge, and velocity.

611 Comparing 2D and 3D models highlights the effectiveness of the 3D model in replicating
612 complex hydrodynamics within the estuary, particularly in capturing the current recirculation and
613 turbulence at the tidal junction of Île d'Orléans. 2DH results synthesized by the 3D model reproduced
614 well the observation provided by the 2DH model. However, the study highlights the importance of
615 considering the vertical velocity component, emphasizing its relevance in comprehending lateral
616 circulation dynamics. The non-uniformity of velocities and the anisotropic nature of flow patterns,
617 coupled with a strong bathymetric gradient, pointed out the very complex and non-linear interaction
618 between tidal and fluvial forcings in the confluence/diffluence junction zone. The nonstationary nature
619 of these mixing phenomena highlights the necessity of employing 3D modeling for a comprehensive
620 spatio-temporal analysis.

621 The observed hysteresis effect, where the flow persists in a certain direction beyond changes in
622 tidal direction, is an important feature captured by the 3D numerical model. This phenomenon,
623 particularly noticeable during transitional phases between ebb and flood tides, demonstrates the complex
624 and dynamic nature of tidal and fluvial interactions. Furthermore, the observed differences in behavior
625 between the north and south branches around the island are explained by local topography and geometry.
626 This heterogeneity plays a fundamental role in shaping estuarine processes, highlighting the importance
627 of accurate and detailed 3D modeling approaches for studying such environments.

628 The integration of 3D numerical results provides a more comprehensive understanding of the
629 hydrodynamic behaviors within the Saint Lawrence River estuary. Beyond confirming and reinforcing
630 pre-existing 2D modeling results, the 3D approach also facilitates cross-analysis between 1D, 2DH, and
631 2DV outcomes, incorporating the vertical velocity component, detailing secondary or recirculating
632 flows and turbulent quantities for different tidal phases. In particular, the vertical velocity distribution
633 enables a deeper understanding of the flow patterns related to steep bathymetric gradients and flow
634 bifurcations with high curvatures. These are essential ingredients for capturing adequately the dynamic
635 of horizontal recirculations and the secondary flows. Their evolution during a tidal phase shows a strong
636 variability in location, size and direction with a hysteretic behavior for both the northern and southern
637 branches at the Y-junction of Île d'Orléans. Furthermore, the 3D model allows for a more precise
638 representation of how site-specific geometry influences hydrodynamic circulation. This includes
639 complex features such as the concave shape of the southern shore, the tip of Île d'Orléans, and the abrupt
640 bathymetric differences between the navigation channel and the southern shore plateau. Moreover, from
641 the fully validated 3D model it is now possible to address climate change issues. For example, future

studies could investigate how the hysteresis and turbulent phenomena or the space-time lag between the north and south channels or the deep channel and the shallow bank will be affected by a modification of the tidal regime. The effects of atmospheric forcing (pressure, wind) and the coupling of the model with ice dynamics could also be explored in future studies, providing further insights into the hydrodynamics of the SLFE responses to seasonal and long-term variations.

Additionally, new detailed field data from a campaign conducted in 2023, with more frequent and closely spaced velocity measurements, could be fully leveraged in the future to offer new insights in the SLFE's dynamics. The numerical model could serve as a physical interpolator, improving or validating the spatiotemporal interpolations mandatory for understanding complex circulation phenomena and optimizing the efficiency of costly field campaigns.

It is commonly stated that 3D modeling is necessary when there are gradients of salinity/density and stratification. This aspect will be the subject of future work. In a future study, it would be interesting to see if/how downstream salinity influences currents and water levels in the upstream freshwater region. This is an interesting research question that would merit further investigation. However, it is important to emphasize that even in a river-estuary section composed entirely of freshwater, 3D modeling can be essential for capturing certain transient tidal and recirculation phenomena related to the complex geometry of estuaries.

Finally, the 3D numerical model provides a solid foundation in hydrodynamics, supporting future studies on transport and mixing phenomena within the SLFE. The inclusion of 3D turbulent processes is crucial for accurately predicting salinity, sediment transport, stratification, chemical compound movement, all of which are key indicators of environmental quality and ecosystem health. This integrated approach allows for comprehensive analysis of water quality, including the dispersion and transport of solid particles such as sediment, micro/nanoplastic, and oil pollution, as well as resilience to episodic pollution events. By incorporating vertical velocity components and turbulence analysis, future research can assess how currents and turbulence patterns influence pollutant spread, identifying accumulation hotspots and high-risk areas. Coupling hydrodynamics with oil pollution transport analyses will offer new insights into the fate and behavior of oil spills within estuaries, aiding in evaluating potential impacts on water quality and ecosystems. Furthermore, understanding hydrodynamic processes will enable the assessment of their effects on stratification mechanisms, turbidity maximum dynamics, and mixing patterns, which are likely to evolve in the face of climate change.

Acknowledgements: The authors would like to thank the Natural Science and Engineering Research Council of Canada (NSERC-Discovery grant RGPIN-2018-0677 and NSERC-Discovery grant RGPIN-2024-03882), the Fonds de Recherche du Québec and the Agence Nationale de la Recherche (FRQ-

ANR, project Emphase, n° 280266) for providing the funding necessary for this publication. The authors extend special thanks to Compute Canada (contract SINAPSE No. 3148 and contract ESPRILE No. 4516) for providing access to the computing facility.

7. References

[1] L. Hu, J. Xu, J. Han, and L. Wang, "Three-Dimensional Hydrodynamics and Morpho-dynamics at a Tidal River Junction", *Estuaries and Coasts*, 2023, doi: 10.1007/s12237-023-01299-3.

[2] F. A. Buschman, M. Van Der Vegt, A. J. F. Hoitink, and P. Hoekstra, "Water and suspended sediment division at a stratified tidal junction", *Journal of Geophysical Research: Oceans*, vol. 118, nº 3, p. 1459-1472, 2013, doi: 10.1002/jgrc.20124.

[3] J. F. Cheylus and Y. Ouellet, "Étude du modèle mathématique de la propagation des marées dans le fleuve St-Laurent : Application du modèle mathématique et étude de la région de l'Ile d'Orléans", Université de Laval, Civil Engineering Department, 1971.

[4] M. I. El-Sabh and T. S. Murty, "Mathematical Modelling of Tides in the St. Lawrence Estuary", in *Oceanography of a Large-Scale Estuarine System*, Silverberg., vol. 39, Springer-Verlag, 1990, p. 10-50.

[5] E. R. Funke and N. L. Crookshank, "A Hybrid Model of the St. Lawrence River Estuary", in *Coastal Engineering*, Hamburg, Germany: American Society of Civil Engineers, 1978, p. 2855-2869. doi: 10.1061/9780872621909.177.

[6] G. Godin, "The Propagation of Tides up Rivers With Special Considerations on the Upper Saint Lawrence River", *Estuarine, Coastal and Shelf Science*, vol. 48, nº 3, p. 307-324, 1999, doi: 10.1006/ecss.1998.0422.

[7] J. W. Kamphuis, "Mathematical model study of the propagation of tides in teh St. Lawrence estuary", National Council of Canada, Hydraulics section, 1968.

[8] *Risque relatif de contamination par région lors de déversements d'hydrocarbures dans le golfe du Saint-Laurent*. Mont-Joli (Québec): Pêches et Océans Canada = Fisheries and Oceans Canada, 2020.

[9] L. Levesque, T. S. Murty, and M. I. El-Sabh, "Numerical Modeling of Tidal Propagation in the St. Lawrence Estuary", *The International Hydrographic Review*, 1979, https://journals.lib.unb.ca/index.php/ihr/article/view/23645

[10] C. Marche et H. W. Partenscky, "Etude de la déformation progressive de l'onde de marée dans l'Estuaire du Saint-Laurent", Université de Montréal. Ecole Polytechnique, Section hydraulique, Montréal, Report, 1974.

[11] B. Morse, "St. Lawrence River Water-levels Study Application of the ONE-D Hydrodynamic Model", Waterways Development Division, Canadian Coast Guard, 1990.

[12] H. W. Partenscky and J. C. Warmoes, "Etude des marées dans l'estuaire du Saint-Laurent entre l'île Anticosti et le lac Saint-Pierre", National Research Council of Canada. Ecole polytechnique (Montréal, Québec). Division d'hydraulique., 1969.

[13] D. Prandle, "Combined one and two dimensional mathematical model of the St. Lawrence river", National Research Council Canada, Canadian Hydraulics Centre, Canada, LTR-HY-13, 1970.

[14] D. Prandle and N. L. Crookshank, "Numerical Model of St. Lawrence River Estuary", *Journal of the Hydraulics Division*, vol. 100, nº 4, p. 517-529, 1974, doi: 10.1061/JYCEAJ.0003930.

[15] S. Robert, D. Plotte, J.-C. Rassam, R. Boivin, R. Larivière, and R. Hausser, "Study of the hydraulic regime of the St. Lawrence River between Montreal and the city of Québec", *Canadian Journal of Civil Engineering*, vol. 19, nº 1, p. 78-85, 1992, doi: 10.1139/l92-008.

[16] D. Bourgault and V. G. Koutitonsky, "Real-time monitoring of the freshwater discharge at the head of the St. Lawrence Estuary", *Atmosphere-Ocean*, vol. 37, nº 2, p. 203-220, 1999, doi: 10.1080/07055900.1999.9649626.

[17] H. W. Partenscky and L. Louchard, "Etude de la variation cyclique de la salinité moyenne dans l'estuaire du Saint-Laurent", Université de Montréal. Ecole Polytechnique, Section hydraulique, 1967.

[18] W. D. Forrester, "Currents and geostrophic currents in the St. Lawrence estuary", Bedford Institute of oceanography, Dartmouth, Canada, Technical Report, 1967.

[19] K.-T. Tee and T.-H. Lim, "The freshwater pulse—a numerical model with application to the St. Lawrence Estuary", *Journal of Marine Research*, vol. 45, nº 4, p. 871-909, 1987, doi: 10.1357/002224087788327127.

[20] C. De Borne De Grandpré, M. I. El-Sabh, and J. C. Salomon, "A two-dimensional numerical modelof the vertical circulation of tides in the St. Lawrence estuary", *Estuarine, Coastal and Shelf Science*, vol. 12, nº 4, p. 375-387, 1981, doi: 10.1016/S0302-3524(81)80002-3.

[21] M. Leclerc, J.-F. Bellemare, and S. Trussard, "Simulation hydrodynamique de l'estuaire supérieur du fleuve Saint-Laurent (Canada) avec un modèle aux éléments finis couvrant–découvrant", *Canadian Journal of Civil Engineering*, vol. 17, nº 5, p. 739-751, 1990, doi: 10.1139/l90-087.

[22] L. Levesque, "Etude du modèle mathématique de la propagation des marées dans l'estuaire du Saint-Laurent", Université du Québec à Rimouski, section d'océanographie, Rimouski, Cahier d'information 2, 1977.

[23] R. D. Pingree and D. K. Griffiths, "A numerical model of the M2 tide in the Gulf of St. Lawrence", *Oceanologica*, vol. 3, nº 2, p. 221-225, 1980.

[24] P. Matte, "Modélisation hydrodynamique de l'estuaire fluvial du Saint-Laurent", Doctoral thesis, Université du Québec Institut National de la Recherche Scientifique Centre Eau Terre Environnement, Québec, 2014.

[25] S. Abair, A. Hammouti, J. Noman, S. Daniel, and D. Pham Van Bang, "Data Capitalization on the December 23, 2022, Storm Surge in Quebec City: Enhancing Coastal Flood Forecasting", *Natural Hazards*, in revision.

[26] A. Cornett and T. Faure, "Assessment of Hydrokinetic Energy Resources in the St Lawrence River and Estuary", International Association for Hydro-Environment Engineering and Research, Hague, Nethelands, 2015.

[27] T. Browne, I. Vouk, A. Cornett, D. Watson, E. Murphy, and M. Sayed, Numerical Simulation of Ice Dynamics on the St. Lawrence River at Montréal, Proceedings of the 20th Workshop on the Hydraulics of Ice Covered Rivers, Ottawa, 2019.

[28] M. Gagnon, "Modélisation tridimensionnelle des courants de marée et de densité dans l'estuaire du Saint-Laurent par la méthode des éléments finis.", Université Laval, 1994.

[29] F. J. Saucier and J. Chassé, "Tidal circulation and buoyancy effects in the St. Lawrence Estuary", *Atmosphere-Ocean*, vol. 38, nº 4, p. 505-556, 2000, doi: 10.1080/07055900.2000.9649658.

[30] F. J. Saucier, F. Roy, D. Gilbert, P. Pellerin, and H. Ritchie, "Modeling the formation and circulation processes of water masses and sea ice in the Gulf of St. Lawrence, Canada", *Journal of Geophysical Research: Oceans*, vol. 108, nº C8, 2003, doi: 10.1029/2000JC000686.

[31] F. Saucier *et al.*, "Modélisation de la circulation dans l'estuaire et le golfe du Saint-Laurent en réponse aux variations du débit d'eau douce et des vents", *Revue des sciences de l'eau / Journal of Water Science*, vol. 22, nº 2, p. 159-176, 2009, doi: 10.7202/037480ar.

[32] R. D. Simons, S. G. Monismith, F. J. Saucier, L. E. Johnson, and G. Winkler, "Modelling stratification and baroclinic flow in the estuarine transition zone of the St. Lawrence estuary", *Atmosphere-Ocean*, vol. 48, nº 2, p. 132-146, 2010, doi: 10.3137/OC316.2010.

[33] "Atlas des courants de marée du Canada. L'estuaire du Saint-Laurent (du cap de Bon Désir jusqu'à Trois-Rivières", Service hydrographique du Canada, 2, 2008.

[34] V. T. Nguyen, "Three-Dimensional Numerical Simulation of Nonlinear Internal Waves in the St. Lawrence Estuary, Canada", *Journal of Coastal Research*, vol. 75, nº sp1, p. 902-906, 2016, doi: 10.2112/SI75-181.1.

[35] D. Lavoie *et al.*, "Large-Scale Atmospheric and Oceanic Control on Krill Transport into the St. Lawrence Estuary Evidenced with Three-Dimensional Numerical Modelling", *Atmosphere-Ocean*, vol. 54, nº 3, p. 299-325, 2016, doi: 10.1080/07055900.2015.1082965.

[36] S. St-Onge-Drouin, G. Winkler, J.-F. Dumais, and S. Senneville, "Hydrodynamics and spatial separation between two clades of a copepod species complex", *Journal of Marine Systems*, vol. 129, p. 334-342, 2014, doi: 10.1016/j.jmarsys.2013.07.014.

[37] J. Urrego-Blanco and J. Sheng, "Study on subtidal circulation and variability in the Gulf of St. Lawrence, Scotian Shelf, and Gulf of Maine using a nested-grid shelf circulation model", *Ocean Dynamics*, vol. 64, nº 3, p. 385-412, 2014, doi: 10.1007/s10236-013-0688-z.

[38] K. Ohashi and J. Sheng, "Influence of St. Lawrence River discharge on the circulation and hydrography in Canadian Atlantic waters", *Continental Shelf Research*, vol. 58, p. 32-49, 2013, doi: 10.1016/j.csr.2013.03.005.

[39] K. Ohashi and J. Sheng, "Investigating the Effect of Oceanographic Conditions and Swimming Behaviours on the Movement of Particles in the Gulf of St. Lawrence Using an Individual-Based Numerical Model", *Atmosphere-Ocean*, vol. 54, nº 3, p. 278-298, 2016, doi: 10.1080/07055900.2015.1090390.

[40] J.-P. Paquin *et al.*, "A new high-resolution Coastal Ice-Ocean Prediction System for the East Coast of Canada", All Depths/Numerical Models/Shelf Seas/Sea and ice/Coastal protection, preprint, 2023. doi: 10.5194/egusphere-2023-42.

[41] S. St-Onge Drouin *et al.*, "Assessment of port ocean prediction system developed under Canada's Oceans Protection Plan: St. Lawrence Estuary.", DFO Canadian Science Advisory Secretariat, Canada, Research Document, in press 2024.

[42] P. Matte, Y. Secretan, and J. Morin, "Temporal and spatial variability of tidal-fluvial dynamics in the St. Lawrence fluvial estuary: An application of nonstationary tidal harmonic analysis", *Journal of Geophysical Research: Oceans*, vol. 119, nº 9, p. 5724-5744, 2014, doi: 10.1002/2014JC009791.

[43] P. Matte, Y. Secretan, and J. Morin, "Hydrodynamic Modeling of the St. Lawrence Fluvial Estuary. II: Reproduction of Spatial and Temporal Patterns", *Journal of Waterway, Port, Coastal, and Ocean Engineering*, vol. 143, nº 5, p. 04017011, 2017b, doi: 10.1061/(ASCE)WW.1943-5460.0000394.

[44] R. Dumasdelage and O. Delestre, "Simulating coliform transport and decay from 3D hydrodynamics model and in situ observation in Nice area", *SN Applied Sciences*, vol. 2, nº 8, p. 1348, 2020, doi: 10.1007/s42452-020-3122-4.

[45] J. A. Graham, D. Haverson, and J. Bacon, "Modelling pollution dispersal around Solomon Islands and Vanuatu", *Marine Pollution Bulletin*, vol. 150, p. 110589, 2020, doi: 10.1016/j.marpolbul.2019.110589.

[46] L.-A. Van, K.-D. Nguyen, F. Le Marrec, and A. Jairy, "Development of a Tool for Modeling the Fecal Contamination in Rivers with Turbulent Flows—Application to the Seine et Marne Rivers (Parisian Region, France)", *Water*, vol. 14, nº 8, p. 1191, 2022, doi: 10.3390/w14081191.

[47] R. D. Simons, S. G. Monismith, L. E. Johnson, G. Winkler, and F. J. Saucier, "Zooplankton retention in the estuarine transition zone of the St. Lawrence Estuary", *Limnology and Oceanography*, vol. 51, nº 6, p. 2621-2631, 2006, doi: 10.4319/lo.2006.51.6.2621.

[48] K. Glock, M. Tritthart, H. Habersack, and C. Hauer, "Comparison of Hydrodynamics Simulated by 1D, 2D and 3D Models Focusing on Bed Shear Stresses", *Water*, vol. 11, nº 2, Art. nº 2, 2019, doi: 10.3390/w11020226.

[49] N. Huybrechts, C. Villaret, and J.-M. Hervouet, "Comparison between 2D and 3D modelling of sediment transport: application to the dune evolution, River Flow, Karlsruhe: Dittrich, Koll, Aberle & Geisenhainer, 2010, p. 887-894.

[50] H. A. M. Al-Zubaidi and S. A. Wells, "Comparison of a 2D and 3D Hydrodynamic and Water Quality Model for Lake Systems", p. 74-84, 2018, doi: 10.1061/9780784481400.007.

[51] M. Ishikawa *et al.*, "Effects of dimensionality on the performance of hydrodynamic models for stratified lakes and reservoirs", *Geoscientific Model Development*, vol. 15, nº 5, p. 2197-2220, 2022, doi: 10.5194/gmd-15-2197-2022.

[52] T. Kesler, "Comparing 1D, 2D, and 3D Hydraulic Models in Urban Flooding Applications", *All Graduate Theses and Dissertations, Spring 1920 to Summer 2023*, 2023, doi: https://doi.org/10.26076/38b6-8acb.

[53] E. Kasvi *et al.*, "Two-dimensional and three-dimensional computational models in hydrodynamic and morphodynamic reconstructions of a river bend: sensitivity and functionality", *Hydrological Processes*, vol. 29, nº 6, p. 1604-1629, 2015, doi: 10.1002/hyp.10277.

[54] L. Chunhui, P. Xishan, K. Jie, and D. Xiaotian, "Comparison of 2D and 3D Models of Salinity Numerical Simulation", *Polish Maritime Research*, vol. 22, 2015, doi: 10.1515/pomr-2015-0028.

[55] W.-B. Chen, W.-C. Liu, and M.-H. Hsu, "Comparison of ANN approach with 2D and 3D hydrodynamic models for simulating estuary water stage", *Advances in Engineering Software*, vol. 45, nº 1, p. 69-79, 2012, doi: 10.1016/j.advengsoft.2011.09.018.

[56] P. Matte, Y. Secretan, and J. Morin, "Hydrodynamic Modeling of the St. Lawrence Fluvial Estuary. I: Model Setup, Calibration, and Validation", *Journal of Waterway, Port, Coastal, and Ocean Engineering*, vol. 143, nº 5, p. 04017010, 2017a, doi: 10.1061/(ASCE)WW.1943-5460.0000397.

[57] P. Matte, Y. Secretan, and J. Morin, "Quantifying lateral and intratidal variability in water level and velocity in a tide-dominated river using combined RTK GPS and ADCP measurements", *Limnology & Ocean Methods*, vol. 12, nº 5, p. 281-302, 2014, doi: 10.4319/lom.2014.12.281.

[58] A. Bouchard and J. Morin, "Reconstitution des débits du Fleuve Saint-Laurent entre 1932 et 1998", Environnement Canada, Service météorologique du Canada, Monitoring et Technologies, Section Hydrologie, Technical Report RT-101, 2000.

[59] M. I. El-Sabh and N. Silverberg, Éd., *Oceanography of a large-scale estuarine system: the St. Lawrence*. in Coastal and estuarine studies, no. 39. Berlin ; New York: Springer-Verlag, 1990.

[60] J.-C. Dionne, "Érosion récente du schorre supérieur à Sainte-Anne-de-Beaupré, Québec", *gpq*, vol. 54, nº 1, p. 69-89, 2002, doi: 10.7202/004792ar.

[61] C. T. Friedrichs and D. G. Aubrey, "Non-linear tidal distortion in shallow well-mixed estuaries: a synthesis", *Estuarine, Coastal and Shelf Science*, vol. 27, nº 5, p. 521-545, 1988, doi: 10.1016/0272-7714(88)90082-0.

[62] J. Morin, P. Boudreau, Y. Secretan, and M. Leclerc, "Pristine Lake Saint-François, St. Lawrence River: Hydrodynamic Simulation and Cumulative Impact", *Journal of Great Lakes Research*, vol. 26, nº 4, p. 384-401, 2000, doi: 10.1016/S0380-1330(00)70702-7.

[63] A. Cornett, A. Pilechi, and J. Cousineau, "Modelling stratified flows in the Saguenay Fjord with TELEMAC-3D", Canadian Hydrotechnical Conference, 2017.

[64] S. Defontaine, "Structure saline, circulation et transport des sédiments en suspension dans un estuaire à coin salé chenalisé : L'estuaire de l'Adour", Doctoral thesis, Pau, 2019. https://www.theses.fr/2019PAUU3022

[65] A. T. K. Do, N. Huybrechts, A. Sottolichio, and A. Gardel, "Modeling and Quantification of Patterns of Salinity, Mixing and Subtidal Flow in the Maroni Estuary", in *APAC 2019*, N. Trung Viet, D. Xiping, et T. Thanh Tung, Éd., Singapore: Springer Singapore, 2020, p. 657-664. doi: 10.1007/978-981-15-0291-0_90.

[66] C. L. Normant, "Three-dimensional modelling of cohesive sediment transport in the Loire estuary", *Hydrological Processes*, vol. 14, nº 13, p. 2231-2243, 2000, doi: 10.1002/1099-1085(200009)14:13<2231::AID-HYP25>3.0.CO;2-#.

[67] D. Pham Van Bang, N. V. Phan, S. Guillou, and K. D. Nguyen, "A 3D Numerical Study on the Tidal Asymmetry, Residual Circulation and Saline Intrusion in the Gironde Estuary (France)", *Water*, vol. 15, nº 23, p. 4042, 2023, doi: 10.3390/w15234042.

[68] S. Ricci, A. Piacentini, A. Weaver, R. Ata, and N. Goutal, "A Variational Data Assimilation Algorithm to Estimate Salinity in the Berre Lagoon with Telemac3D", TELEMAC-MASCARET User Conference, 2013, p. 19-24.

[69] P. Santoro, M. Fossati, P. Tassi, N. Huybrechts, D. Pham Van Bang, and J. C. I. Piedra-Cueva, "A coupled wave–current–sediment transport model for an estuarine system: Application to the Río de la Plata and Montevideo Bay", *Applied Mathematical Modelling*, vol. 52, p. 107-130, 2017, doi: 10.1016/j.apm.2017.07.004.

[70] C. E. Stringari, W. C. Marques, L. F. De Mello, and R. T. Eidt, "Application of telemac - ecos modeling system at the southern brazilian shelf: case study of Tramandaí beach oil spill", *Marine Systems & Ocean Technology*, vol. 9, nº 2, p. 105-112, 2014, doi: 10.1007/BF03449291.

[71] L. Troudet and S. Desmare, "Modélisation hydrodynamique sur le littoral de la Région des Pays-de-la-Loire", in *XIIIèmes JNGCGC (Journées Nationales Génie Cotier - Génie Civil), Dunkerque*, Paralia, 2014, p. 185-194. doi: 10.5150/jngcgc.2014.021.

[72] J.-M. Hervouet, *Hydrodynamics of free surface flows: modelling with the finite element method*. Chichester: Wiley, 2007.

[73] J.-M. Hervouet, C. Denis, and E. David, "Revisiting the Thompson boundary conditions. In: Violeau, Damien; Hervouet, Jean-Michel; Razafindrakoto, Emile; Denis, Christophe (Hg.): Proceedings of the XVIIIth Telemac & Mascaret User Club 2011", EDF R&D, Chatou. Chatou: EDF R&D, 2011.

[74] K. W. Thompson, "Time dependent boundary conditions for hyperbolic systems.", *Journal of Computational physics*, nº 68, p. 1-24, 1987.

[75] M. Hurtado-Herrera, M. Uh Zapata, A. Hammouti, D. Pham Van Bang, W. Zhang, and K. D. Nguyen, "Numerical investigation of the scour around a diamond-and square-shaped pile in a narrow channel", *Ocean Engineering*, vol. 309, nº 1, doi: 10.1016/j.oceaneng.2024.118374.

[76] P. Matte, Y. Secretan, and J. Morin, "Drivers of residual and tidal flow variability in the St. Lawrence fluvial estuary: Influence on tidal wave propagation", *Continental Shelf Research*, vol. 174, p. 158-173, 2019, doi: 10.1016/j.csr.2018.12.008.

[77] K. Shiono and D. W. Knight, "Turbulent open-channel flows with variable depth across the channel", *Journal of Fluid Mechanics*, vol. 222, nº 1, p. 617, 1991, doi: 10.1017/S0022112091001246.

Highlights

Investigation of 3D circulation and secondary flows in the St. Lawrence Fluvial Estuary at a tidal junction

Maëlys le Mouel, Pascal Matte, Abdelkader Hammouti, Damien Pham Van Bang

- New 3D numerical model of the St. Lawrence estuary
- Flow reversal and turbulence during flood/ebb cycle for spring/neap tide in a tidal junction
- Current recirculation and phase delay between shallow bank and deep channel

Declaration of interests

☐ The authors declare that they have no known competing financial interests or personal relationships that could have appeared to influence the work reported in this paper.

☒ The authors declare the following financial interests/personal relationships which may be considered as potential competing interests:

Damien Pham Van Bang reports a relationship with Natural Sciences and Engineering Research Council of Canada that includes: funding grants. If there are other authors, they declare that they have no known competing financial interests or personal relationships that could have appeared to influence the work reported in this paper.